The VWF/LRP4/aVb3-axis represents a novel pathway regulating proliferation of human vascular smooth muscle cells

Jérémy Lagrange, Morel Worou, Jean-Baptiste Michel, Alexandre Raoul, Mélusine Didelot, Vincent Muczynski, Paulette Legendre, François Plénat, Guillaume Gauchotte, Marc-Damien Lourenco-Rodrigues, et al.

The VWF/LRP4/$\alpha_v\beta_3$-axis represents a novel pathway regulating proliferation of human vascular smooth muscle cells

Jérémy Lagrange[#1], Morel E. Worou[#1], Jean-Baptiste Michel[2], Alexandre Raoul[1], Mélusine Didelot[1], Vincent Muczynski[3], Paulette Legendre[3], François Plénat[4], Guillaume Gauchotte[5], Marc-Damien Lourenco-Rodrigues[3], Olivier D. Christophe[3], Peter J. Lenting[3], Patrick Lacolley[1], Cécile V. Denis*[3], Véronique Regnault*[1]

[1] INSERM, UMR_S 1116, Vandœuvre-lès-Nancy, France; Université de Lorraine, DCAC, Nancy, France.

[2] INSERM, UMR_S 1148, LVTS, Université de Paris, France

[3] HITh, UMR_S1176, INSERM, Université Paris-Saclay, 94276, Le Kremlin-Bicêtre, France

[4] Université de Lorraine, Nancy, France.

[5] CHRU, Anatomie et cytologie pathologiques, Nancy, France

[#] Jérémy Lagrange and Morel E. Worou participated equally to this work.

* Véronique Regnault and Cécile V. Denis participated equally to this work.

Short title: VWF induces VSMC proliferation

Corresponding author:

Cécile V. Denis, Inserm U1176, 80 rue du Général Leclerc, 94276 Le Kremlin-Bicêtre cedex

cecile.denis@inserm.fr

Category: Vascular Pathophysiology

Abstract count: 286

Word count: 9051

Figures: 8

References: 43

Abstract:

Aims: Von Willebrand factor (VWF) is a plasma glycoprotein involved in primary hemostasis, while also having additional roles beyond hemostasis namely in cancer, inflammation, angiogenesis and potentially in vascular smooth muscle cell (VSMC) proliferation. Here, we addressed how VWF modulates VSMC proliferation and investigated the underlying molecular pathways and the *in vivo* pathophysiological relevance.

Methods and results: VWF induced proliferation of human aortic VSMCs and also promoted VSMC migration. Treatment of cells with a siRNA against α_v integrin or the RGT-peptide blocking $\alpha_v\beta_3$ signaling abolished proliferation. However, VWF did not bind to $\alpha_v\beta_3$ on VSMCs through its RGD-motif. Rather, we identified the VWF A2 domain as the region mediating binding to the cells. We hypothesized the involvement of a member of the LDL-related receptor protein (LRP) family due to their known ability to act as co-receptors. Using the universal LRP-inhibitor receptor-associated protein, we confirmed LRP-mediated VSMC proliferation. siRNA experiments and confocal fluorescence microscopy identified LRP4 as the VWF-counterreceptor on VSMCs. Also co-localization between $\alpha_v\beta_3$ and LRP4 was observed via proximity ligation analysis and immuno-precipitation experiments. The pathophysiological relevance of our data was supported by VWF-deficient mice having significant reduced, if any, hyperplasia in carotid artery ligation and artery femoral denudation models. In wild-type mice, infiltration of VWF in intimal regions enriched in proliferating VSMCs was found. Interestingly, also analysis of human atherosclerotic lesions showed abundant VWF accumulation in VSMC-proliferating rich intimal areas.

Conclusions: VWF mediates VSMC proliferation through a mechanism involving A2 domain binding to the LRP4 receptor and integrin $\alpha_v\beta_3$ signaling. Our findings provide new insights into the mechanisms that drive physiological repair and pathological hyperplasia of the arterial vessel wall. In addition, the VWF/LRP4-axis may represent a novel therapeutic target to modulate VSMC proliferation.

Translational perspective

The mechanisms that drive physiological repair and pathological hyperplasia of the arterial vessel wall are complex and only partially understood. Specifically, the role of subendothelial-matrix proteins remains unclear. Here, we show that the hemostatic protein von Willebrand factor (VWF) accumulates in the vascular wall of atherosclerotic lesions and localizes to areas of vascular smooth muscle cell (VSMC) proliferation. VWF was found to use its A2-domain for binding to the VSMC-receptor LRP4, which in turn triggered outside-in signaling via integrin $\alpha_V\beta_3$, thereby inducing VSMC proliferation. Interfering with A2-domain/LRP4 interactions might offer innovative and additional therapeutical approaches to limit pathological hyperplasia.

1. Introduction

Vascular smooth muscle cells (VSMCs) are crucial to maintain the structure and functions of the arterial wall. Upon vascular injury, however, these cells may start to proliferate and migrate from the media into the intima in an early process of repair called neointima formation or intimal hyperplasia (IH). This process is key in several physiological and pathogenic events, such as atherosclerosis progression and in-stent restenosis[1-3]. The molecular basis of VSMC proliferation is complex and may be provoked by a number of mitogenic agents or growth factors, such as platelet-derived growth factor (PDGF)[4]. A basic requirement for these growth factors to induce VSMC proliferation involves their translocation from circulating blood into the vascular wall. Interestingly, the vascular wall already consists of many matrix proteins, and the mitogenic potential of these matrix proteins has poorly been explored so far.

One protein known to be present constitutively in the subendothelial matrix is von Willebrand factor (VWF). VWF is a multimeric plasma glycoprotein that plays a crucial role in hemostasis, bridging platelets to subendothelial components upon vascular injury, thus contributing to bleeding arrest[5]. Following its biosynthesis by endothelial cells, VWF is directed towards storage organelles, the Weibel-Palade bodies, from where it will be secreted through constitutive or regulated pathways[6]. The constitutive pathway not only releases VWF towards the luminal side but also serves to deposit VWF in the subendothelium, usually into an acellular area[7].

Animal studies from the 1990s suggested that the location and quantity of VWF in the vessel wall can vary in vascular pathologies. Indeed, in a model of cuff-induced neointima formation in the rabbit carotid artery, VWF accumulates in the media after 24h, while at later time-points (7-14 days), VWF deposits were observed in the extracellular space of the neointima between VSMCs[8]. Additional modifications in VWF deposition in the vessel wall, whether in the media or during neointima thickening have been reported in various animal models of atherosclerosis or angioplasty[9-11]. These observations have raised the question of a potential role for VWF in vascular tissue injury responses in general and in modulating VSMC behavior in particular. An attempt to answer this question was undertaken by Qin *et al* who reported decreased IH following carotid artery ligation in a murine strain known to have low VWF levels, the RIIIS/J mice, in comparison to wild-type C57B/6J mice[12]. Additional studies further demonstrated that VWF can interact directly with murine VSMCs, and induces proliferation of these cells[12-15]. The VWF-induced proliferation of murine VSMCs has been proposed to involve a Notch-dependent signaling pathway[13-15].

Apparently, VWF combines its presence in the vascular wall with the potential to modulate VSMC proliferation. However, the molecular basis of VWF-mediated VSMC proliferation remains obscure. We further do not know whether the link between VWF and VSMCs applies to human VSMC patho-physiology as well.

Here, we explored human atherosclerotic tissue at different stages of severity, observing abundant intimal VWF accumulation in aorta, coronary and carotid atherothrombotic lesions. In addition, we demonstrate that human VSMCs are prone to VWF-induced proliferation via a novel and unusual pathway. First, the VWF A2-domain induced proliferation via interactions with low-density lipoprotein receptor-related protein-4 (LRP4), a newly identified receptor for VWF. Second, LRP4 was found to co-localize with integrin $\alpha_V\beta_3$, and VWF binding to LRP4 triggered an outside-in signaling pathway via integrin $\alpha_V\beta_3$.

2. Methods

Additional information on Methods is available in the online Supplementary materials.

2.1 Materials and reagents

A detailed description of resources used in this study (reagents & cells, antibodies, inhibitors) are detailed (name, vendor/source and clone/reference) in the Supplementary materials and methods.

2.2 Animals

8-10 weeks old wild-type (VWF+/+) or VWF-deficient (VWF-/-)[16] male mice on a C57BL/6J background were used for this study. Housing and experiments were conducted in accordance with the French regulations and the experimental guidelines of the European Community (Directive 2010/63/EU). Animals were housed under standard conditions and given free access to standard rodent chow and water. The protocols were approved by the local Animal Ethics Committee of the University of Lorraine, France (#9411-2017032718404787 v4). Anesthesia was induced by isoflurane inhalation at 3.5% in 1L/min oxygen, and then maintained at 1.5% in 1L/min oxygen during the intervention. Mice were euthanized via exsanguination under isoflurane anesthesia (1.5% in 1L/min oxygen).

2.3 Human tissues

Post-mortem human arterial, aortic, carotid and coronary artery walls, including healthy and pathology at different stages of atherosclerotic diseases were collected from the Inserm human CV biobank (BB-0033-00029, U 1148, X. Bichat hospital, Paris), included in the European network BBMRI-ERIC, in accordance with the French regular and ethical rules (BioMedicine Agency convention DC2018-3141) and the principles of the declaration of Helsinki. Approval was obtained from the French Biomedical Agency (ABM, PFS09-007 & PFS17-002) and the Institutional Ethical Review board (SC09-09-66). Tissues were obtained from deceased organ donors for kidney and/or hepatic transplantation, in the absence of therapeutic uses for the aorta and/or the heart. Human arterial tissues were fixed with 4% (w/v) buffered formaldehyde solution prepared by depolymerization of paraformaldehyde and imbedded in paraffin. Serial 5-7 μm thick sections were performed.

2.4 Immunohistochemistry

For VSMC detection in murine tissue sections, representative sections were immunostained with a monoclonal antibody (MoAb) against α Smooth Muscle Actin (α-SMA), a MoAb against VWF or a MoAb against proliferating cell nuclear antigen (PCNA). Briefly, sections were deparaffinized and rehydrated. Endogenous peroxidases were quenched with 3% H_2O_2. The mouse primary antibody was first combined with a secondary antibody (a goat anti-mouse

antibody conjugated to horse-radish peroxidase (HRP)) in a tube and allowed sufficient time to form an antibody complex. Any non-complexed secondary antibody was bound up with mouse serum. The mixture is then applied to the tissue. After washing, sections were successively incubated with a biotinylated secondary antibody for 30 min at RT, washed, and reacted with HRP-streptavidin. Color development from peroxidase antibodies was carried out using 3,3'-diaminobenzidine as the chromogen.

Immunohistochemistry of human arterial tissues were performed using α-SMA and VWF MoAbs and then revealed using 3,3'-diaminobenzidine staining on serial sections.

2.5 Cell culture

Human aortic VSMCs were obtained as cryopreserved ampules from Lonza (cat# CC-2571), containing ≥500,000 cells/ampule with >95% viability and >95% seeding efficiency. All cells were from single individuals aged between 18 and 57 years, and >10 different lots have been used during the study (ratio male/female about 60:40). Human aortic VSMCs were cultured in Smooth Muscle Cell Growth Medium-2 (SmGM-2) containing 5% fetal bovine serum at 37°C with 5% CO_2. Human VSMCs were used between passages 3 and 6.

2.6 Proliferation assay

Human VSMCs were seeded at a density of $5x10^4$ cells/well in SmGM-2 containing 5% fetal bovine serum into a 24-well plate. The next day, cells were synchronized in serum-free medium for 6h (or 24h or 48h for indicated experiments) and treated with various proteins: recombinant human platelet-derived growth factor (PDGF-BB), VWF (0-4 nM) or recombinant VWF-Fc fragments (100 ng/ml) in serum-free medium. After 24h, cell proliferation was evaluated by cell counting using a Neubauer-improved counting chamber (Marienfeld). Alternate methods to assess cell proliferation such as analysis of cellular DNA content by flow cytometry or incorporation of 5-bromo-2'-deoxyuridine (BrdU) were used for some experiments. In indicated groups, cells were pre-incubated with receptor-associated protein (RAP; 1 µM) for 1 min, a cyclic RGDPV peptide (1 mM) or RGT and GRT peptides (250 µM) for 30 min. Some experiments were performed in the presence of antibody LM609 (10 µg/ml). In the control group, VSMCs were cultured without any treatment. For each experiment, triplicate wells were counted.

2.7 Wound-healing and migration assays

Experiments were performed on confluent monolayers of human VSMCs seeded in a 6-well plate. After starving the cells in serum-free medium for 6h, a wound scratch was created with a 200 µl pipette tip. Cells were washed twice with PBS to remove detached cells, and then cultured in a serum-free medium with or without VWF or VWF fragment. The wounded area

was observed and photographed at t=0,16, 24 and 48h after wounding. Using ImageJ Software, VSMC migration and wound repair was evaluated by the number of cells that migrated into the wounded area.

2.8 Western blotting

Cells treated as indicated in individual experiments were harvested, washed twice with PBS and lysed in a cold lysis buffer (Roche Life Sciences, Meylan France) containing proteases and phosphatase inhibitors cocktails (Roche). The lysates were pelleted and the supernatant fractions were collected and examined for protein concentration using a Bradford Protein assay kit (Bio-Rad, Marnes-la-Coquette, France). Proteins were separated by SDS-PAGE and electro-transferred onto a nitrocellulose membrane. After blocking for 1h in 5% non-fat milk dissolved in Tris buffered saline with 0.1% Tween-20, membranes were incubated with indicated specific primary antibodies overnight at 4°C. Membranes were then washed and incubated with appropriate secondary antibodies for 1h at room temperature (RT). The immunoreactive bands were visualized by chemiluminescence (Western ECL substrate, Bio-Rad) using a luminescent image analyzer system (LAS-4000 mini, Fujifilm).

2.9 Immunofluorescence staining of VSMCs

A detailed description of this procedure is presented in the Supplementary materials. VSMCs were grown on glass coverslips, and incubated in the presence or absence of VWF. After formaldehyde fixation, cells were incubated with primary antibodies against VWF, $\alpha_v\beta_3$ integrin, Protease Activated Receptor-2 (PAR2) or LRP4. Nuclei were counterstained with 4',6'-diamidino-2-phenylindole (DAPI). Negative controls were performed by omitting the primary antibody or the VWF treatment. Images were acquired via fluorescent confocal microscopy, and analyzed by Image J software using the plugin *colocalization finder* to calculate the Pearson's coefficient[17].

For the Duolink®- Proximity Ligation Assay (PLA), double immunostaining of human VSMCs (treated or not with VWF) was performed using primary antibodies to LRP4 and $\alpha_v\beta_3$ integrin, the secondary antibodies being replaced by PLA probes. The remainder of the protocol was conducted according to the manufacturer's recommendations. For confocal microscopy, a Nikon C2 microscope with Ti-FL stage and C-HGFi fluorescent bulb was used. Acquisition was performed with the NiS Elements software.

2.10 siRNA transfection

To evaluate the role of LRP4 or $\alpha_v\beta_3$ in VWF-induced human VSMC proliferation, cells were transfected with siRNA directed against LRP4 or α_v or the negative control using a magnet-assisted transfection reagent according to the manufacturer's instructions. siRNA-sequences

are provided in the Supplementary materials. Briefly, for each well of a 24-well plate, 0.25 μg of siRNA was diluted in serum-free Dulbecco's Modified Eagle Medium (DMEM) to an end volume of 50 μl. The diluted siRNA was added to 0.75 μl of MATra-Si Reagent, followed by mixing and incubation at RT for 20 min. The transfection complex siRNA/MATra-Si reagent was added to the cells. The plate was then incubated on a magnetic plate for 15 min at 37°C. The magnetic plate was removed, followed by a 24h resting period in a serum-free medium. Cells were then used for VWF-induced human VSMCs proliferation or migration assays.

2.11 Binding assays

LRP proteins (50 µl, 1 µg/ml) were immobilized on half-well microtiter plates in carbonate buffer pH 9.6 overnight at 4°C. After washing with TBS (Tris 25 mM, NaCl 150 mM, pH 7.4) containing 2.5 mM $CaCl_2$ and 0.1% Tween-20, a post-coat step was applied (30 min at 37°C in the same buffer but with 3% BSA). VWF or VWF fragments diluted in TBS-Ca-Tween/3% BSA were then added to the wells (50 µl) for 2h at 37°C. In one set of experiments, VWF was pre-incubated or not with 1 mg/ml of ristocetin at RT before addition to the wells. After three washes, HRP-coupled antibodies to VWF or to Fc-tag were added (50 µl) for 2h at 37°C. 3,3',5,5'-tetramethylbenzidine was added to reveal bound proteins and the reaction was stopped with H_2SO_4. OD was read at 450 and 570 nm in a multiplate reader (Biotek).

2.12 Statistical analysis

Data are presented as mean±SD, unless specified. Statistical analysis was performed using Graphpad prism 5 software. A two-tailed unpaired Student *t* test was applied for comparisons between two groups. When indicated, multiple t-test was performed. One-way ANOVA followed by Tukey's or Dunnett's multiple comparisons test was performed when comparing multiple groups. $P<0.05$ was considered as statistically significant. For the *in vivo* experiments, an N-1 Chi-square test was performed when comparing the number of mice with or without hyperplasia. When comparing the intima/media ratio or nuclei number, a Mann-Whitney test was applied.

3. Results

3.1 VWF is involved in intimal hyperplasia in vivo

In view of the different mouse strains that were compared for their sensitivity to VWF-dependent hyperplasia formation in previous studies[12], we first set to confirm such an effect in a more appropriate setting using VWF-KO mice and their wild-type littermates. Two distinct models of vascular injury were used: 1) ligation of the common carotid artery and 2) femoral artery denudation. In the carotid artery ligation model, 5 out of 9 VWF+/+ mice had extensive intimal hyperplasia (IH), whereas none of the 8 VWF-/- did (p=0.015; **Supplementary Table S1**). A similar difference in neointima formation was observed in the femoral artery denudation model, with 10 out of 14 VWF+/+ mice developing IH versus 4 out of 13 VWF-/- mice (p=0.038; **Supplementary Table S1 & Fig. S1**). Histological analysis of the ligated and contralateral arteries revealed the presence of neointima selectively in the ligated arteries of VWF+/+ mice (**Fig. 1A**). Importantly, only the neointima of ligated arteries in VWF+/+ mice stained positive for PCNA, a marker for cell proliferation (**Fig. 1B**). Indeed, the intima/media ratio was significantly increased in these mice (p=0.0294), as was the number of nuclei (p=0.0294; **Fig. 1F**). Neointima stained positive for α-SMA, compatible with proliferating cells being VSMCs (**Fig. 1C**). Interestingly, neointima also stained positive for VWF, which was absent in the intima of the contralateral artery, suggesting that VWF is present within the proliferating area (**Fig. D**). This infiltration seemed specific for VWF as no changes were observed for collagen, another sub-endothelial matrix protein (**Fig. 1E**). Thus, these mouse data confirm the link between VWF and VSMC proliferation. However, it does not teach us whether VWF modulates VSMC proliferation in a direct or indirect manner.

3.2 VWF is present in the intima and core of human atherosclerotic lesions

To explore the possibility that VWF could contribute to the pathogenesis of neointima formation in humans, we performed qualitative analyses of rare tissue aortic sections for the presence of VWF in areas enriched in proliferating VSMCs. As expected, VWF is predominantly detected in the most luminal part of healthy human aorta (corresponding to the endothelium), with minor variable subendothelial staining in the α-SMA-positive cell area (**Fig. 2A**). In contrast, clear prominent VWF immunostaining was observed in the intima of human fatty streaks (aorta and coronary artery), largely overlapping with areas of α-SMA-positive cell migration and potential proliferation (**Fig. 2B** & **Supplementary Fig. S2**). Similarly, abundant VWF immunostaining was detected in endothelium and VSMC-rich subendothelium of the cap in human fibrolipidic plaques (**Fig. 2C**). VWF accumulation also predominated in the core of the plaque, an area of high plasma protein insudation (**Fig. 2C**). Another example relates to complex neo-atherosclerotic lesions that are formed following coronary artery stenting. Also in this condition,

VWF accumulates in the VSMC-rich area of the shoulder of a stented segment (**Supplementary Fig. S2**).

Extravascular VWF accumulation was also observed in carotid tissue sections (**Supplementary Fig. S2**). Profuse VWF immunostaining was present in areas of carotid intimal proliferation, involving both endothelial, subendothelial and SMA-positive intima (**Supplementary Fig. S2**). In culprit plaque, VWF appeared in the cap endothelium and in the VSMC-rich cap intimal proliferation area (**Supplementary Fig. S2**). As observed in the fibrolipidic aorta, VWF is also present in the VSMC-poor external part of the lesion, an area corresponding to intraplaque hemorrhage (**Supplementary Fig. S2**). Altogether, we observe an accumulation of VWF in VSMC-rich areas of various pathological arterial tissue sections. It seems conceivable therefore that VWF may be in direct contact with these cells.

3.3 VWF induces human aortic VSMC proliferation and migration

In the remainder of our study, we focused on the potential of VWF to induce proliferation of human VSMCs and its underlying molecular pathway. In a first series of experiments, the mitogenic effect of VWF on VSMCs was compared to that of PDGF-BB. Proliferation in the absence of any mitogenic protein was arbitrarily defined as 1.0. As expected, PDGF-BB induced VSMC proliferation in a dose-dependent manner (**Fig. 3A**). In line with previous studies, the proliferative effect of PDGF-BB followed a bell-shaped curve[18, 19]. A similar dose-dependent and bell-shaped effect was observed for VWF (**Fig. 3A**). Interestingly, similar maximum proliferative index values were obtained for PDGF-BB and VWF (1.8±0.1 for PDGF-BB *vs* 1.8±0.3 for VWF at the peak, $p<0.0005$ *vs* untreated cells). Similar proliferative index values for VWF were obtained when applying other means to quantify cell proliferation: cell cycle analysis by flow cytometry or incorporation of BrdU (**Fig. 3B**). In an alternative approach, we analyzed the effect of VWF on VSMC recolonization in a wound healing scratch assay, which measures both migration and proliferation. Again, VWF was found to stimulate VSMC recolonization of the wound area as indicated by the significantly higher number of cells present after 16, 24 and 48h (**Supplementary Fig. S3**). These data are compatible with VWF having the potential to simulate human VSMC proliferation, akin to PDGF-BB.

3.4 Signaling pathways associated with VWF-induced VSMC-proliferation

We next explored the cellular responses of VSMCs used at passages 3-6, following exposure to VWF. First, quantitative PCR of nine specific VSMC markers was performed at 24h and 48h after exposure to VWF. However, no change in RNA expression for each of these markers was detected compared to cells without VWF exposure (**Fig. 3C**). In accordance with these data, no changes in expression of α-SMA, Smooth Muscle Myosin Heavy Chain (SM-MHC), vimentin, myocardin, and smoothelin upon VWF treatment were observed (**Supplementary**

Fig. S4), indicating the maintenance of a differentiated state of VSMCs, allowing the proliferative status of the cells.

To analyze which signaling pathways were activated by VWF, we quantified phosphorylation of Akt, ERK1/2, p38-Mitogen-activated protein kinases (p38-MAPK), Src and STAT3. No VWF-dependent activation of STAT3 could be detected (**Supplementary Fig. S5**). In contrast, VWF significantly induced Akt phosphorylation at the Thr308 site and ERK1/2 phosphorylation at the Thr202/Tyr204 site with a maximum effect at 15 min (**Fig. 3D-E**). To further elucidate the VWF-dependent signaling pathway upstream of regulators of Akt and ERK1/2, we examined the level of phosphorylation of p38-MAPK and Src, a major intracellular mediator of integrin-dependent functions. Induction of both p38-MAPK phosphorylation at the Thr179/Tyr181 site and Src phosphorylation at the Tyr418 site were increased within 5 to 15 min and the phosphorylation returned to basal levels after 30 min (**Fig. 3F-G**).

3.5 Identification of $\alpha_v\beta_3$ involvement in VWF-induced VSMC proliferation

The $\alpha_v\beta_3$ integrin has previously been reported as a receptor for VWF on VSMCs[15], and we therefore investigated whether VWF co-localized with this integrin at the cellular surface *via* confocal microscopy. VSMCs were incubated in the absence or presence of VWF and co-stained for α_V and VWF (**Fig. 4A**) or, as negative control, PAR2 and VWF (**Fig. 4B**). Confocal images revealed selective co-staining for VSMCs incubated with VWF and co-stained for α_V and VWF, but not in other conditions (**Fig. 4A-B**). Observations were quantified via pixel-analysis of multiple z-stacks, revealing a median Pearson's correlation coefficient of 0.71 for α_V/VWF versus 0.11 for PAR2/VWF (**Fig. 4A-B**). These data confirm that VWF co-localizes with $\alpha_V\beta_3$.

To establish if VWF-induced VSMC proliferation involves $\alpha_v\beta_3$, we used a siRNA-strategy. A specifically designed α_v-targeting siRNA blocked α_v RNA expression by 78% and protein expression by 41%, whereas both remained unchanged in the presence of control siRNA (**Supplementary Fig. S6**). Adding the α_v siRNA and control siRNA to VSMCs induced a 15-20% reduction in cell proliferation in the absence of VWF ($p=0.012$ and $p=0.046$, respectively when comparing to "no VWF no siRNA" condition; **Fig. 4C**), indicating that the siRNA procedure in itself has a minor but significant effect on VSMC proliferation. However, a similar 1.6-fold increase in VSMC proliferation was observed for both control conditions (no siRNA and control siRNA) in the presence of VWF compared to the absence of VWF, showing that this procedure does not interfere with the mitogenic activity of VWF. In contrast, no VWF-induced proliferation was found in the presence of the α_v siRNA (**Fig. 4C**). Apparently, the presence of $\alpha_V\beta_3$ is indispensable for VWF-induced VSMC proliferation.

3.6 The VWF-$\alpha_v\beta_3$ integrin axis in VSMC proliferation

Since VWF comprises an RGD-motif in its C-terminal region, we anticipated that this motif would mediate direct binding of VWF to $\alpha_v\beta_3$. This hypothesis was challenged by analyzing VWF-mediated VSMC proliferation in the absence or presence of a cRGDPV-peptide or the anti-$\alpha_v\beta_3$ integrin antibody LM609, both of which would annihilate the binding of the VWF RGD motif to $\alpha_v\beta_3$ and subsequent VSMC proliferation. In the absence of VWF, we observed that the cRGDPV-peptide alone inhibited basal cell proliferation by 60% (p=0.002 compared to control without any additions), whereas no effect was observed when antibody LM609 was tested in the absence of VWF (**Fig. 4D**). Despite the inhibitory effect of the cRGDPV-peptide on basal VSMC proliferation, a similar VWF-dependent increase in VSMC proliferation was observed in all three conditions: 1.5-fold, 1.6-fold and 1.7-fold for control, the cRGDPV-peptide and antibody LM609, respectively.

We next explored the option whether the observed VWF-dependent effect involves $\alpha_v\beta_3$-mediated signaling. This was tested using a myristoylated RGT-peptide (myr-RGT), which selectively inhibits β_3 outside-in signaling[21]. As control, its myristoylated GRT-control peptide (myr-GRT) was applied[21]. Neither peptide had any influence on basal VSMC proliferation, nor did the myr-GRT-control peptide affect VWF-induced proliferation (**Fig. 4E**). In contrast, the myr-RGT-peptide proved an efficient inhibitor of VWF-enhanced VSMC proliferation (proliferative index 2.1±0.2 without peptide *vs* 0.9±0.2 with peptide, p<0.0001; **Fig. 4E**). We then hypothesized that should the VWF mitogenic effect involves signaling via $\alpha_v\beta_3$, then the down-regulation of $\alpha_v\beta_3$ expression would result in an absence of phosphorylation of downstream kinases. Human VSMCs were therefore treated with α_v siRNA and its effect on Src phosphorylation was evaluated. Whereas VWF induced Src phosphorylation in VSMCs treated with control siRNA, this was completely abolished in cells treated with α_v siRNA (**Supplementary Fig. S7**). Thus, VWF induces an $\alpha_v\beta_3$-dependent signaling pathway that results in phosphorylation of Src-kinase. In contrast, this process proceeds independently of a direct interaction between VWF and the RGD-responsive site in $\alpha_v\beta_3$.

3.7 Identification of a member of the LRP family as crucial determinant for VWF-induced VSMC proliferation

Since $\alpha_v\beta_3$ is seemingly not the primary VWF receptor in our experiments, it is conceivable that a second receptor able to crosstalk with $\alpha_v\beta_3$ is implicated. LRP family members are known co-receptors in different cell types, including VSMCs. Indeed, a cooperation between LRP1 and $\alpha_v\beta_3$ in response to tissue-type plasminogen activator has been reported[22]. We therefore tested whether an LRP receptor was involved, and GST-RAP was used as general inhibitor of the LRP-receptor family. GST-RAP alone had no effect on basal VSMC proliferation (**Fig. 5A**).

However, its presence completely abolished VWF-induced cell proliferation (proliferation index with VWF alone: 2.2±0.2 *vs* 0.7±0.2 with VWF+GST-RAP, p<0.0001; **Fig. 5A**). We also measured proliferation using a combination of both GST-RAP and myr-RGT. Blocking simultaneously $\alpha_v\beta_3$ and LRP had no additional effect and VWF-induced VSMC proliferation was reduced to basal proliferation (**Fig. 5A**), suggesting that both receptors operate in concert. We considered the possibility that the LRP-receptor involved in this VWF-dependent process would be LRP1, previously recognized as receptor for VWF on macrophages, and also known to be expressed on VSMCs[23, 24]. However, for this interaction, VWF requires to adopt an active, platelet-binding conformation, which can be mimicked by pre-incubating VWF with ristocetin[23]. Unexpectedly, pre-treatment of VWF with ristocetin did not further increase the proliferative index at any of the VWF concentrations tested (**Fig. 5B**), suggesting that another LRP family member rather than LRP1 is involved in VWF-dependent VSMC proliferation.

3.8 VWF A2-domain mediates VSMC proliferation

To narrow our search for an LRP family member as potential receptor for VWF on VSMCs, we decided to investigate the molecular determinants on the VWF subunit, necessary to induce VSMC proliferation. To do so, we used purified recombinant VWF domains. The VWF mature subunit with its domain structure is represented on **Fig. 5C**. Among isolated VWF fragments, only the VWF-A2 domain promoted VSMC proliferation. No significant difference with full-length VWF were observed in terms of proliferative index (2.1±0.2 for VWF, 1.7±0.5 for A2-Fc, *p*=0.47; **Fig. 5D**). All other VWF fragments as well as a control Fc-fused unrelated protein (Siglec5-Fc) proved inefficient in promoting cell proliferation. A dimeric D4-CK fragment containing the VWF RGD-motif (within the C4 domain) also did not show any proliferative effect, compatible with the finding that the VWF-mediated effect is independent of its RGD-motif (**Fig. 5D**). In the wound healing scratch assay, VWF-A2 fragment induced VSMC migration, similar to full-length VWF (**Fig. 5E & Supplementary Fig. S8**). Similar to full-length VWF, A2-Fc induced proliferation was completely abolished in the presence of the LRP-inhibitor GST-RAP or the presence of myr-RGT (**Fig. 5F**). In addition, A2-Fc induced similar signaling as full-length VWF, as illustrated by the phosphorylation of Erk1/2 (**Fig. 5G**). Apparently, the A2-Fc protein mimics full-length VWF not only in inducing VSMC proliferation and migration, but also in doing so via an LRP-triggered outside-in signaling pathway involving $\alpha_v\beta_3$.

3.9 VWF binds to LRP4 on VSMCs to induce cell proliferation

Having identified an LRP receptor as counter-receptor for the VWF A2-domain on VSMCs, we next attempted to pinpoint which LRP member was involved. First, we measured VWF binding, in the absence of ristocetin, to different LRP receptors selected on the basis of mRNA

identification in VSMCs (www.proteinatlas.org). In these conditions, no binding of VWF to LRP1, LRP5 or LRP8 was detected. However, VWF displayed strong binding to LRP4 in the absence of ristocetin (**Fig. 6A**). Furthermore, when testing VWF-Fc fragments, we observed a specific interaction between VWF-A2 domain and LRP4 (**Fig. 6B**), thus suggesting that LRP4 could represent a candidate receptor for VWF on VSMCs. Since LRP4 is particularly known for its expression on neurons and skeletal muscle cells rather than VSMCs, we first verified LRP4 expression on VSMCs. To this end, immunofluorescence studies were performed and a strong signal for LRP4 on these cells could be detected (**Fig. 6C**). Moreover, when cells were incubated in the presence of VWF, a clear co-staining between VWF and LRP4 was detected (**Fig. 6D**), suggesting that VWF is able to interact with LRP4 at the cellular surface. Using siRNA against LRP4, we next demonstrated the direct involvement of this receptor in VWF-mediated VSMC proliferation. siRNA directed against LRP4 led to a >90% decrease in mRNA expression and a 40% decrease in protein expression (**Supplementary Fig. S9**). In the proliferation assay, complete inhibition of VWF-induced VSMC proliferation was observed in the presence of the LRP4 siRNA with no significant effect of the control siRNA (proliferative index of 1.7±0.1 with control siRNA *vs* 1.0±0.1 with LRP4 siRNA, $p<0.0001$; **Fig. 6E**). Thus, LRP4 seems to be an essential element in VWF-induced VSMC proliferation.

3.10 LRP4 and $\alpha_v\beta_3$ cooperate to mediate VWF-induced VSMC proliferation

Given the observation that LRP4 and $\alpha_v\beta_3$ seem to mediate VWF-dependent VSMC proliferation in a concerted action (**Fig. 5A**), we explored the option that both receptors would be in close proximity at the cellular surface. To this end, Duolink®-PLA analysis was performed, which detects proteins being located within a range of 40 nm. Whereas negative conditions (single primary with both secondary antibodies) did not reveal any signal, we observed a positive signal in the test conditions, demonstrating that both receptors were within 40 nm of distance, strongly suggesting the existence of an interaction (**Fig. 7A-C**). Indeed, the LRP4/$\alpha_V\beta_3$ complex could be precipitated using anti-α_V antibodies (**Fig. 7D**). Interestingly, while Duolink-PLA analysis suggested reduced interactions between LRP4 and $\alpha_V\beta_3$ in the presence of VWF (**Supplementary Fig. S10**), this was not observed in the immunoprecipitation experiments (**Fig. 7D**). We anticipate that reduced complex formation in the former assay is due to reduced antibody accessibility of the receptors in the presence of VWF.

We also checked whether siRNA against LRP4 abrogated the $\alpha_v\beta_3$-dependent activation of Src phosphorylation by VWF. The LRP4 siRNA completely abolished VWF-induced Src activation compared with the control siRNA (**Fig. 7E-F**). Suppression of Akt, ERK1/2 and p-38 MAPK phosphorylation was also evidenced in the presence of the LRP4 siRNA (**Fig. 7E-F**).

Taken together, we have identified VWF as a mitogenic factor that efficiently induces VSMC proliferation via a previously unrecognized pathway involving the heterologous receptor complex LRP4/ $\alpha_v\beta_3$, which in turn activates a Src-mediated signaling cascade.

4. Discussion

Besides its well-known function in primary hemostasis, VWF is increasingly recognized as a pleiotropic protein involved in processes related to angiogenesis, cancer and inflammation[5]. In the vascular wall, observations that VWF location and quantity may vary in vascular diseases indicate a potential intervention of VWF in tissue remodeling following injury[8-11]. In particular, a role for VWF in modulating murine VSMC proliferating properties has been suggested by Qin et al[12]. In this study, we have now characterized this ability of VWF to induce human VSMC proliferation by identifying the pathways involved. We observed a dose-dependent proliferating effect of VWF on VSMCs, consistent with the previous findings. In addition to inducing cell proliferation, VWF also proved able to mediate cell migration in a wound healing scratch assay, further demonstrating its ability to influence tissue remodeling. VWF-induced proliferation and migration of VSMCs had no effect on their differentiation, in agreement with the current concept that dedifferentiation is not a prerequisite for VSMC proliferation[25, 26]. Finally, involvement of the ERK1/2-MAPK cascade and Akt signaling pathway completed and supported the picture of a proliferating status of the VSMCs in presence of VWF.

Having established this proliferating effect of VWF, our next step consisted in identifying the cellular receptor(s) involved. Based on our knowledge of the receptor repertoire of VSMCs, we first considered $\alpha_v\beta_3$ integrin as a potential candidate. Indeed this integrin is strongly expressed by VSMCs[27], is a known receptor for VWF[28] and is involved in VSMC proliferation and migration[29]. Our initial experiments showing co-localization of $\alpha_v\beta_3$ and VWF at the surface of VSMCs supported this hypothesis. Further confirmation of $\alpha_v\beta_3$ involvement arose from the complete inhibition of the VWF-proliferative effect upon treatment of the cells with siRNA against α_v. Importantly, on VSMCs the α_v subunit is only associated to β_3 and β_3 is only associated to α_v[27]. Blocking $\alpha_v\beta_3$ signaling using the myr-RGT-peptide[21, 30] also completely annihilated VWF-induced cell proliferation. However, the use of inhibitors of $\alpha_v\beta_3$ engagement[31] such as a cyclic RGD peptide or the LM609 antibody did not block VWF-mediated cell proliferation. Altogether, our results emphasize the critical importance of $\alpha_v\beta_3$-dependent signaling in mediating VWF-induced cell proliferation, a process that seems to occur independently of VWF binding to this integrin.

Since members of the LRP family are known to act as co-receptors in a variety of cellular settings, including VSMCs[22], we hypothesized for such a mechanism and indeed, using the LRP-inhibitor GST-RAP, we exposed the importance of an LRP receptor in VWF-induced VSMC proliferation. Among LRP family members, VWF is known to bind LRP1 but this binding involves its A1 domain and requires VWF to be in an active conformation[6, 23]. Our present observations showing a lack of effect of ristocetin, a VWF activator, added to the identification of the A2 domain as the necessary VWF determinant, thus pointed to an LRP member other than LRP1. Our data identified LRP4 as a new receptor for VWF. Indeed, using direct binding

experiments we showed that LRP4 is the only LRP member potentially present on VSMCs that is able to bind VWF without ristocetin. In addition, we showed that the only VWF region able to substitute for full-length VWF in mediating VSMC proliferation and migration, *i.e.* the A2 domain is also able to bind to LRP4. Using immunofluorescence, we confirmed expression of LRP4 by VSMCs and showed colocalization between LRP4 and VWF. And finally, direct evidence of LRP4 involvement came from the use of siRNA against LRP4, which completely blocked VWF-induced proliferation.

Three important and original pieces of information can be highlighted from these experiments. The first one is the involvement of the VWF-A2 domain. Besides its critical role in harboring binding and cleavage sites for ADAMTS13, the enzyme responsible for regulating VWF multimeric size[32], the A2 domain has not been reported to play a major role in mediating VWF interaction with its numerous partners. This is in contrast to its neighboring domains, which contains binding sites for many VWF ligands such as glycoprotein Ib, heparin, sulfatides, collagen VI for the A1 domain [33, 34] and collagens for the A3 domain[35]. However very recently, a study reported an interaction between the VWF A2 domain and extracellular vimentin[36], suggesting that the importance of this domain has not yet been fully investigated. The second original finding relates to LRP4. This member of the LRP family has been first identified in 1998 and is unique among other LRP receptors since it is the only type II transmembrane receptor, with its N-terminal region located within the cytoplasmic side of the plasma membrane[37]. A complete deficiency of LRP4 is incompatible with life in mice[38]. LRP4 has been reported to be involved in multiple functions: on skeletal muscle cells, LRP4 is crucial for the formation of neuromuscular junction[39] while on non-muscle cells, LRP4 plays a role in presynaptic differentiation or in bone-mass homeostasis[40]. Although the main functions of the LRP receptors appear to be related to cargo transport or internalization of macromolecules, LRP4 mostly serves as a signal transducer or modulator. A number of ligands for LRP4 have already been identified and for each of its functions, an original and complex signaling mechanism has been described[39]. Our results appear to be following a similar trend. Indeed, LRP4 appears to be the receptor for VWF at the cell surface and as such, it could potentially signal directly through Ca2+/calmodulin-dependent protein kinase II (CaMKII) to activate ERK1/2, Akt and p38-MAPK. However, in our conditions, an LRP4-mediated outside-in signaling through $\alpha_v\beta_3$ is necessary to induce VSMC proliferation, suggesting cooperation between both receptors, the third important point in our study. Indeed, we were able to show using immunoprecipitation experiments and the Duolink-PLA that LRP4 and $\alpha_v\beta_3$ are co-localizing at the surface of VSMCs. Furthermore, the use of siRNA against one or the other of these receptors completely abrogates the proliferating effect of VWF, highlighting the physiological relevance of this cooperation. It is not unusual for LRP receptors to associate with co-receptors depending on the cellular environment, allowing them to extend their ligand profile, to modulate their cellular

activities and to enable signal transduction[41]. This capacity makes LRP family members very versatile receptors and multifunctional cell-surface proteins. For example, cooperation between LRP1 and $\alpha_v\beta_3$ has been shown to mediate vasocontraction of VSMCs by tissue-type plasminogen activator[22]. Still on VSMCs, LRP1 appears to control PDGF receptor-dependent signaling pathways, controlling cell proliferation and preventing atherosclerosis[24].

Relevant to our findings is of course its physiological context. Our mouse model based on a full deficiency of VWF displayed a strong reduction in neointima formation in two different experimental approaches for intimal hyperplasia, consistent with observations using a mouse with a partial deficiency of VWF[12]. In addition, infiltration of VWF in regions enriched in proliferating VSMCs was detected in wild-type mice. It should be noted that both mouse models are limited in that they do not distinguish between a direct and indirect role of VWF. VWF may affect VSMC proliferation indirectly via several mechanisms. For instance, endothelial cells lack VWF-specific storage organelles (Weibel-Palade bodies) in VWF-/- mice[16], which could negatively impact the release of necessary growth factors or other proteins essential in the process to induce VSMC proliferation. However, Weibel-Palade bodies are normally present in the endothelial cells of the RIIIS/J-mice, which express low levels of VWF[12]. It is unlikely therefore that the lack of neointima formation in the VWF-/- mice is due to the absence of Weibel-Palade bodies. Alternatively, VWF may be necessary for the recruitment of platelets at the site of injury, which can release growth factors contributing to cell proliferation. However, characterization of the model by Roque *et al* revealed an early-stage (1h) accumulation of platelets at the site of injury without the need for VWF[42], arguing for a similar platelet involvement between VWF+/+ and VWF-/- mice. Finally, VWF has recently been reported to contribute to wound healing, acting as a molecular bus to deliver growth factors to wound sites[43]. It is possible that this mechanism contributes to the *in vivo* VWF-mediated VSMC proliferation, existing in parallel to the LRP4-$\alpha_v\beta_3$ mechanism that we describe here.

In view of our findings and the potential mechanism by which VWF contributes to VSMC proliferation, it seems relevant to distinguish between subendothelial VWF and VWF derived from the circulation. The data observed using human atherosclerotic pathology fit well with the hypothesis that VWF is present in the wall proportional to the pathology intensity, mainly in endothelium and intima but also in the core of the lesion. These data suggest that deposition of VWF originates from endothelial cells surrounding the lesion. However, other areas in the atherosclerotic lesion, predominantly in the core of the plaque, are prone to hemorrhages and plasma protein insudation[20]. It is likely that in these plasma-borne atheroma injuries, plasma-derived VWF participates in the arterial cellular responses.

In conclusion, we have observed the combined presence of VWF and VSMCs in the neointima of various pathological arteries, but not healthy vessels. In addition, we found that VWF is an effective mitogenic agent towards VSMCs, and further analysis revealed a novel, previously

unrecognized molecular pathway underlying this mitogenic action. VWF can induce VSMC proliferation, involving cooperation between two receptors, one important for ligand binding (LRP4) and the second for signal transduction ($\alpha_v\beta_3$). Our findings provide new insights into the mechanisms that drive physiological repair and pathological hyperplasia of the arterial vessel wall. The identification of VWF and LRP4 may therefore be of potential interest in prevention and treatment of arterial wall remodeling, and open avenues for novel therapeutical strategies.

6. Acknowledgements

We wish to thank Dr. Huguette Louis and Mrs Kenza Benkirane for expert technical assistance. We are indebted to Dr. Muriel Laffargue for her willingness to share her team's expertise in performing femoral wire injury in mice. We thank the Flow cytometry Core Facility and the Imaging Core Facility (PTIBC) of UMS2008/US40 IBSLor (Université de Lorraine-CNRS-INSERM) for cell cycle analysis and confocal microscopy respectively.

7. Sources of funding

This work was supported by the Investments for the Future program under grant agreement No ANR-15-RHU-0004; the Agence Nationale de la Recherche (ANR-13-BSV1-0026); the Région Grand Est; and the "Fonds européen de développement regional".

8. Conflict of interest

None declared.

9. Author contributions

JL, MEW, MD, VM, AR, PL, FP, GG, MDLR, VR performed experiments and analyzed data.
JBM provided human tissue sections and analyzed histology sections.
ODV, PJL, PL, CVD, VR analyzed data, designed and supervised the study.
PJL, PL, CVD, VR wrote the manuscript.
All authors confirmed the final version of the manuscript.

10. Data availability

The data underlying this article will be shared on reasonable request to the corresponding author.

11. References

1. Dzau VJ, Braun-Dullaeus RC, Sedding DG. Vascular proliferation and atherosclerosis: new perspectives and therapeutic strategies. *Nat Med* 2002;**8**:1249-1256.
2. Schober A. Chemokines in vascular dysfunction and remodeling. *Arterioscler Thromb Vasc Biol* 2008;**28**:1950-1959.
3. Lacolley P, Regnault V, Nicoletti A, Li Z, Michel JB. The vascular smooth muscle cell in arterial pathology: a cell that can take on multiple roles. *Cardiovasc Res* 2012;**95**:194-204.
4. Millette E, Rauch BH, Kenagy RD, Daum G, Clowes AW. Platelet-derived growth factor-BB transactivates the fibroblast growth factor receptor to induce proliferation in human smooth muscle cells. *Trends Cardiovasc Med* 2006;**16**:25-28.
5. Lenting PJ, Casari C, Christophe OD, Denis CV. von Willebrand factor: the old, the new and the unknown. *J Thromb Haemost* 2012;**10**:2428-2437.
6. Lenting PJ, Christophe OD, Denis CV. von Willebrand factor biosynthesis, secretion, and clearance: connecting the far ends. *Blood* 2015;**125**:2019-2028.
7. Sporn LA, Marder VJ, Wagner DD. Differing polarity of the constitutive and regulated secretory pathways for von Willebrand factor in endothelial cells. *J Cell Biol* 1989;**108**:1283-1289.
8. Kockx MM, De Meyer GR, Andries LJ, Bult H, Jacob WA, Herman AG. The endothelium during cuff-induced neointima formation in the rabbit carotid artery. *Arterioscler Thromb* 1993;**13**:1874-1884.
9. Bosmans JM, Kockx MM, Vrints CJ, Bult H, De Meyer GR, Herman AG. Fibrin(ogen) and von Willebrand factor deposition are associated with intimal thickening after balloon angioplasty of the rabbit carotid artery. *Arterioscler Thromb Vasc Biol* 1997;**17**:634-645.
10. De Meyer GR, Hoylaerts MF, Kockx MM, Yamamoto H, Herman AG, Bult H. Intimal deposition of functional von Willebrand factor in atherogenesis. *Arterioscler Thromb Vasc Biol* 1999;**19**:2524-2534.
11. Giddings JC, Banning AP, Ralis H, Lewis MJ. Redistribution of von Willebrand factor in porcine carotid arteries after balloon angioplasty. *Arterioscler Thromb Vasc Biol* 1997;**17**:1872-1878.
12. Qin F, Impeduglia T, Schaffer P, Dardik H. Overexpression of von Willebrand factor is an independent risk factor for pathogenesis of intimal hyperplasia: preliminary studies. *J Vasc Surg* 2003;**37**:433-439.
13. Meng H, Zhang X, Lee SJ, Wang MM. Von Willebrand factor inhibits mature smooth muscle gene expression through impairment of Notch signaling. *PLoS One* 2013;**8**:e75808.
14. Zhang X, Meng H, Blaivas M, Rushing EJ, Moore BE, Schwartz J, Lopes MB, Worrall BB, Wang MM. Von Willebrand Factor permeates small vessels in CADASIL and inhibits smooth muscle gene expression. *Transl Stroke Res* 2012;**3**:138-145.
15. Scheppke L, Murphy EA, Zarpellon A, Hofmann JJ, Merkulova A, Shields DJ, Weis SM, Byzova TV, Ruggeri ZM, Iruela-Arispe ML, Cheresh DA. Notch promotes vascular maturation by inducing integrin-mediated smooth muscle cell adhesion to the endothelial basement membrane. *Blood* 2012;**119**:2149-2158.
16. Denis C, Methia N, Frenette PS, Rayburn H, Ullman-Cullere M, Hynes RO, Wagner DD. A mouse model of severe von Willebrand disease: defects in hemostasis and thrombosis. *Proc Natl Acad Sci U S A* 1998;**95**:9524-9529.
17. French AP, Mills S, Swarup R, Bennett MJ, Pridmore TP. Colocalization of fluorescent markers in confocal microscope images of plant cells. *Nat Protoc* 2008;**3**:619-628.
18. Facchiano A, De Marchis F, Turchetti E, Facchiano F, Guglielmi M, Denaro A, Palumbo R, Scoccianti M, Capogrossi MC. The chemotactic and mitogenic effects of platelet-derived growth factor-BB on rat aorta smooth muscle cells are inhibited by basic fibroblast growth factor. *J Cell Sci* 2000;**113 (Pt 16)**:2855-2863.
19. Li H, Papadopoulos V, Vidic B, Dym M, Culty M. Regulation of rat testis gonocyte proliferation by platelet-derived growth factor and estradiol: identification of signaling mechanisms involved. *Endocrinology* 1997;**138**:1289-1298.

20. Michel JB, Virmani R, Arbustini E, Pasterkamp G. Intraplaque haemorrhages as the trigger of plaque vulnerability. *Eur Heart J* 2011;**32**:1977-1985, 1985a, 1985b, 1985c.
21. Su X, Mi J, Yan J, Flevaris P, Lu Y, Liu H, Ruan Z, Wang X, Kieffer N, Chen S, Du X, Xi X. RGT, a synthetic peptide corresponding to the integrin beta 3 cytoplasmic C-terminal sequence, selectively inhibits outside-in signaling in human platelets by disrupting the interaction of integrin alpha IIb beta 3 with Src kinase. *Blood* 2008;**112**:592-602.
22. Akkawi S, Nassar T, Tarshis M, Cines DB, Higazi AA. LRP and alphavbeta3 mediate tPA activation of smooth muscle cells. *Am J Physiol Heart Circ Physiol* 2006;**291**:H1351-1359.
23. Rastegarlari G, Pegon JN, Casari C, Odouard S, Navarrete AM, Saint-Lu N, van Vlijmen BJ, Legendre P, Christophe OD, Denis CV, Lenting PJ. Macrophage LRP1 contributes to the clearance of von Willebrand factor. *Blood* 2012;**119**:2126-2134.
24. Boucher P, Gotthardt M, Li WP, Anderson RG, Herz J. LRP: role in vascular wall integrity and protection from atherosclerosis. *Science* 2003;**300**:329-332.
25. Owens GK, Kumar MS, Wamhoff BR. Molecular regulation of vascular smooth muscle cell differentiation in development and disease. *Physiol Rev* 2004;**84**:767-801.
26. Michel JB. Phylogenic determinants of cardiovascular frailty, focus on hemodynamics and arterial smooth muscle cells. *Physiol Rev* 2020;**in press, doi: 10.1152/physrev.00022.2019**.
27. Lacolley P, Regnault V, Segers P, Laurent S. Vascular Smooth Muscle Cells and Arterial Stiffening: Relevance in Development, Aging, and Disease. *Physiol Rev* 2017;**97**:1555-1617.
28. Denis C, Williams JA, Lu X, Meyer D, Baruch D. Solid-phase von Willebrand factor contains a conformationally active RGD motif that mediates endothelial cell adhesion through the alpha v beta 3 receptor. *Blood* 1993;**82**:3622-3630.
29. Byzova TV, Rabbani R, D'Souza SE, Plow EF. Role of integrin alpha(v)beta3 in vascular biology. *Thromb Haemost* 1998;**80**:726-734.
30. Xi X, Bodnar RJ, Li Z, Lam SC, Du X. Critical roles for the COOH-terminal NITY and RGT sequences of the integrin beta3 cytoplasmic domain in inside-out and outside-in signaling. *J Cell Biol* 2003;**162**:329-339.
31. Mao X, Said R, Louis H, Max JP, Bourhim M, Challande P, Wahl D, Li Z, Regnault V, Lacolley P. Cyclic stretch-induced thrombin generation by rat vascular smooth muscle cells is mediated by the integrin alphavbeta3 pathway. *Cardiovasc Res* 2012;**96**:513-523.
32. Crawley JT, de Groot R, Xiang Y, Luken BM, Lane DA. Unraveling the scissile bond: how ADAMTS13 recognizes and cleaves von Willebrand factor. *Blood* 2011;**118**:3212-3221.
33. Christophe O, Obert B, Meyer D, Girma JP. The binding domain of von Willebrand factor to sulfatides is distinct from those interacting with glycoprotein Ib, heparin, and collagen and resides between amino acid residues Leu 512 and Lys 673. *Blood* 1991;**78**:2310-2317.
34. Sixma JJ, Schiphorst ME, Verweij CL, Pannekoek H. Effect of deletion of the A1 domain of von Willebrand factor on its binding to heparin, collagen and platelets in the presence of ristocetin. *Eur J Biochem* 1991;**196**:369-375.
35. Kalafatis M, Takahashi Y, Girma JP, Meyer D. Localization of a collagen-interactive domain of human von Willebrand factor between amino acid residues Gly 911 and Glu 1,365. *Blood* 1987;**70**:1577-1583.
36. Fasipe TA, Hong SH, Da Q, Valladolid C, Lahey MT, Richards LM, Dunn AK, Cruz MA, Marrelli SP. Extracellular Vimentin/VWF (von Willebrand Factor) Interaction Contributes to VWF String Formation and Stroke Pathology. *Stroke* 2018;**49**:2536-2540.
37. Tomita Y, Kim DH, Magoori K, Fujino T, Yamamoto TT. A novel low-density lipoprotein receptor-related protein with type II membrane protein-like structure is abundant in heart. *J Biochem* 1998;**124**:784-789.
38. Weatherbee SD, Anderson KV, Niswander LA. LDL-receptor-related protein 4 is crucial for formation of the neuromuscular junction. *Development* 2006;**133**:4993-5000.
39. Shen C, Xiong WC, Mei L. LRP4 in neuromuscular junction and bone development and diseases. *Bone* 2015;**80**:101-108.

40. Xiong L, Jung JU, Wu H, Xia WF, Pan JX, Shen C, Mei L, Xiong WC. Lrp4 in osteoblasts suppresses bone formation and promotes osteoclastogenesis and bone resorption. *Proc Natl Acad Sci U S A* 2015;**112**:3487-3492.
41. Nykjaer A, Willnow TE. The low-density lipoprotein receptor gene family: a cellular Swiss army knife? *Trends Cell Biol* 2002;**12**:273-280.
42. Roque M, Fallon JT, Badimon JJ, Zhang WX, Taubman MB, Reis ED. Mouse model of femoral artery denudation injury associated with the rapid accumulation of adhesion molecules on the luminal surface and recruitment of neutrophils. *Arterioscler Thromb Vasc Biol* 2000;**20**:335-342.
43. Ishihara J, Ishihara A, Starke RD, Peghaire CR, Smith KE, McKinnon TAJ, Tabata Y, Sasaki K, White MJV, Fukunaga K, Laffan MA, Lutolf MP, Randi AM, Hubbell JA. The heparin binding domain of von Willebrand factor binds to growth factors and promotes angiogenesis in wound healing. *Blood* 2019;**133**:2559-2569.

12. Figure legends

Figure 1: Immunostaining of murine arterial tissue sections after carotid ligation.

A-E. Arterial tissue sections obtained 4 weeks post-injury from VWF+/+ and VWF-/- mice were stained using HES (A) or Sirius Red (E) or with antibodies against PCNA (B), α-SMA (C) or VWF (D). M: media; I: intima. Scale bars, 50 μm. **F.** Intima/media ratio and nuclei count in injured carotid arteries (n=9 for VWF+/+ and n=8 for VWF-/-). Statistical analysis was performed using a Mann-Whitney test.

Figure 2: Immunostaining of VWF and α-SMA in different stages of aortic atherosclerosis in human.

A. Detection of VWF in endothelium of healthy human aorta and in the subendothelial layer positive for α-SMA staining. **B**. Fatty streaks showing presence of VWF in the α-SMA-positive neointima. **C**. Subendothelium VWF staining in VSMC-rich fibrocellular cap and VWF accumulation in the acellular lipid core of fibrolipidic plaques. Full morphology of the section (Nanozoomer) were associated with X4 magnification (red boxes) and X20 magnification (black boxes). M, media; I, intima. Scale bars = 2 mm (Nanozoomer), 1 mm (X4 magnification) and 0.2 mm (X20 magnification).

Figure 3: VWF-induced proliferation cultured human VSMCs.

A. Human aortic VSMCs were incubated with VWF or PDGF-BB (0-4 nM) for 24h, and cell proliferation was evaluated. Presented is the proliferative index relative to proliferation with medium alone, which is arbitrarily defined as 1.0. Data represent the mean±SEM of 3 (for PDGF) or 4 experiments (for VWF), each performed in triplicate. **B.** Measure of VWF-induced VSMC proliferation using 3 different methods: incorporation of BrdU (n=7), cell counting (n=4) or analysis of cellular DNA (n=3). Data represent mean±SD. **C.** VSMCs were incubated in the absence or presence of VWF (1 nM) for 24h (grey bars) or 48h (dotted bars). RNA was isolated and quantitative PCR was performed for 9 different markers. Relative changes in RNA expression compared to cells incubated in the absence of VWF are presented. Data are expressed as mean±SD, n=indicated for each condition. **D-G**. Phosphorylation of Akt, ERK1/2, p38-MAPK and Src was assessed after exposing cells to 1 nM VWF for 5 to 60 min. Cell lysates were prepared and phosphorylation of Akt (Thr^{308}), ERK1/2 (Thr^{202}/Tyr^{204}), p38-MAPK (Thr^{179}/Tyr^{181}) or Src (Tyr^{418}) was determined using colorimetric cell-based elisa kits. Data represent mean±SD (n=4), and results are expressed as fold increase relative to unstimulated control. Statistical analysis was performed using one-way Anova with Dunnett's multiple comparison.

Figure 4: Involvement of $\alpha_v\beta_3$ in VWF-mediated VSMC proliferation

A-B: Confocal immunostaining of VWF (red) and $\alpha_v\beta_3$ (panel A; green) or PAR2 (panel B; green) in VSMCs incubated for 24h at 37°C in the absence or presence of VWF (1 nM). Nuclei were counterstained using DAPI. Images were acquired using stacks (1 µm) in sequential for the three channels (488, 555 & 633 nm). Bars represent 25 µm, objective 40x. The Pearson's correlation coefficient was obtained by Image J software using the plugin *colocalization finder*. Data are expressed as mean±SD. N=33 cells for α_V without VWF; n=54 for α_V with VWF; n=64 for PAR2 without VWF and n=42 for PAR with VWF. Statistical analysis involved a Mann-Whitney test. **C**. Proliferative index of human VSMCs transfected with control siRNA or siRNA against α_v and incubated with 1 nM VWF for 24h. **D-E**. Proliferative index of human VSMCs treated with VWF (1 nM) for 24h in the presence the LM609 antibody (10 µg/ml) or after pre-treatment of the cells with a cyclic RGDPV peptide (1 mM; panel D) or synthetic myristoylated RGT/GRT peptides (250 µM; panel E). Experiments were reproduced three times in triplicate (C-E) and statistical analysis was performed using one-way Anova with Tukey's multiple comparison.

Figure 5: Identification of the VWF molecular determinant involved in mediating VSMC proliferation. A. Proliferative index of human VSMCs pretreated with GST-RAP (1 µM) or a mixture of GST-RAP and synthetic myristoylated RGT/GRT peptides (250 µM) prior addition of 1 nM VWF for 24h. Data represent mean±SD; n=6 for No VWF, VWF and GST-RAP; n=3 for VWF+GST-RAP, VWF+RGT-myr+GST-RAP and VWF+GRT-myr+GST-RAP (with each experiment performed in triplicate). **B.** Proliferative response of human VSMCs following incubation with VWF or VWF/ristocetin (0-4 nM). Data represent mean±SEM of 3 independent experiments. **C.** Schematic representation of the domain structure of VWF. **D.** Proliferative index of human VSMCs in response to VWF (1 nM), PDGF (0.2 nM) or various VWF-fragments (100 ng/ml) (mean±SD; n is indicated for each condition). **E.** A wound healing scratch assay was performed on human VSMCs in the absence or presence of VWF-A2/Fc (100 ng/ml). Reappearance of cells in the wounded area was monitored at t=0,16, 24 and 48h and quantified using ImageJ Software. Data represent mean±SD (n=3). **F.** Proliferative index of human VSMCs pretreated with GST-RAP (1 µM) or a mixture of GST-RAP and synthetic myristoylated RGT/GRT peptides (250 µM) prior addition of 100 ng/ml VWF-A2/Fc for 24h. **G.** Phosphorylation of ERK1/2 was assessed after exposing cells to 1 nM VWF for 5 to 60 min. Cell lysates were prepared and phosphorylation of ERK1/2 (Thr^{202}/Tyr^{204}) was determined using colorimetric cell-based elisa. Data represent mean±SD (n=4), and results are expressed as fold increase relative to unstimulated control. Statistical analysis was performed using one-way Anova with Tukey's (panels A, D, F) or Dunnett's (panel G) multiple comparison or using multiple t-test (panel E).

Figure 6: Involvement of LRP4 in VWF-mediated VSMC proliferation

A. Immobilized LRP variants (1 µg/ml) were incubated with VWF (0-7.5 µg/ml) in the absence of VWF activator. Bound-VWF was probed by a peroxidase-coupled polyclonal anti-VWF antibody. Data represent mean±SD (n=3). Closed circles: LRP4; open circles: LRP1; open squares LRP5; closed squares LRP8. **B.** Immobilized LRP4 (1 µg/ml) was incubated with VWF-A2/Fc (closed triangles) or VWF-A3/Fc (open triangles; 0-15 µg/ml). Bound-VWF fragments were probed using peroxidase-coupled polyclonal anti-Fc antibodies. Data represent mean±SD (n=3). **C.** Fluorescent immunostaining of LRP4 on VSCMCs. Nuclei were counterstained using DAPI. Representative images were acquired using confocal microscopy. Bars represent 25 µm for objective 40x or 10 µm for objective 100x. **D.** VSMCs incubated in the presence or absence of VWF were stained using anti-LRP4 (green) and anti-VWF (red) antibodies. Nuclei were counterstained using DAPI. Shown are representative merged images acquired using confocal microscopy. Bars represent 25 µm. **E.** Proliferative index of human VSMCs transfected with control siRNA or siRNA against LRP4 and incubated with 1 nM VWF for 24h. Experiment was reproduced three times in triplicate and statistical analysis was performed using one-way Anova with Tukey's multiple comparison.

Figure 7: Association between $\alpha_v\beta_3$ and LRP4 on VSMCs and effect on MAPK signaling pathways

A-C. Duolink-proximity ligation assay (PLA) analysis of LRP4 and $\alpha_v\beta_3$ expression and colocalization on VSMCs. Panels A-B represents control conditions in the presence of only one primary antibody (A: anti-α_V, B: anti-LRP4) and both secondary antibodies with fluorescent probes. Panel C represents test conditions (both primary and secondary antibodies with fluorescent probes). Red spots appear only when $\alpha_v\beta_3$ and LRP4 are within a distance of ≤40 nm. Nuclei were counterstained with DAPI. Scale bars: 10µm, Objective 63x. **D.** VSMCs incubated in the presence or absence of VWF were lysed, and immunoprecipitated using anti α_V-antibodies or control antibodies. Western blots of lysates were first stained using anti α_V-antibodies and subsequently with anti-LRP4 antibodies. **E-F.** Phosphorylation of Akt, ERK1/2, p38-MAPK and Src was assessed after exposing cells transfected with control or siRNA against LRP4 to 1 nM VWF for 10 min. Cell lysates were prepared and phosphorylation of Akt (Thr^{308}), ERK1/2 (Thr^{202}/Tyr^{204}), p38-MAPK (Thr^{179}/Tyr^{181}) or Src (Tyr^{418}) was determined by Western blotting. Immunoreactive bands were visualized by chemiluminescence and quantified using a luminescent image analyzer system. Data represent mean±SD (n=3) and results are expressed as fold increase relative to unstimulated control. Statistical analysis was performed using t-test.

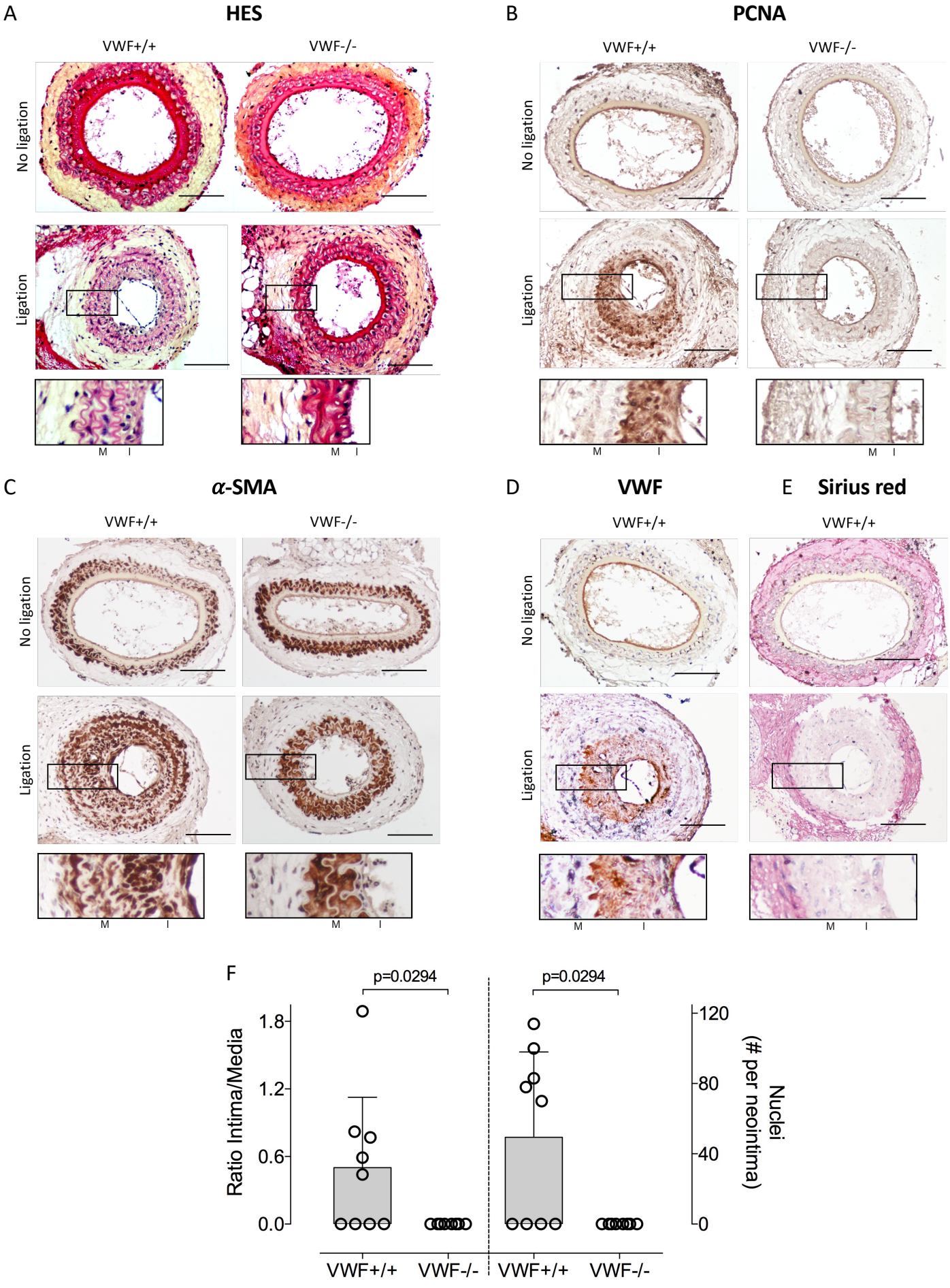
A
HES
VWF+/+
VWF-/-
No ligation
Ligation
M
I
B
PCNA
VWF+/+
VWF-/-
No ligation
Ligation
M
I
C
α-SMA
VWF+/+
VWF-/-
No ligation
Ligation
M
I
D
VWF
VWF+/+
No ligation
Ligation
M
I
E
Sirius red
VWF+/+
M
I
F
p=0.0294
p=0.0294
Ratio Intima/Media
1.8
1.2
0.6
0.0
120
80
40
0
Nuclei
(# per neointima)
VWF+/+
VWF-/-
VWF+/+
VWF-/-

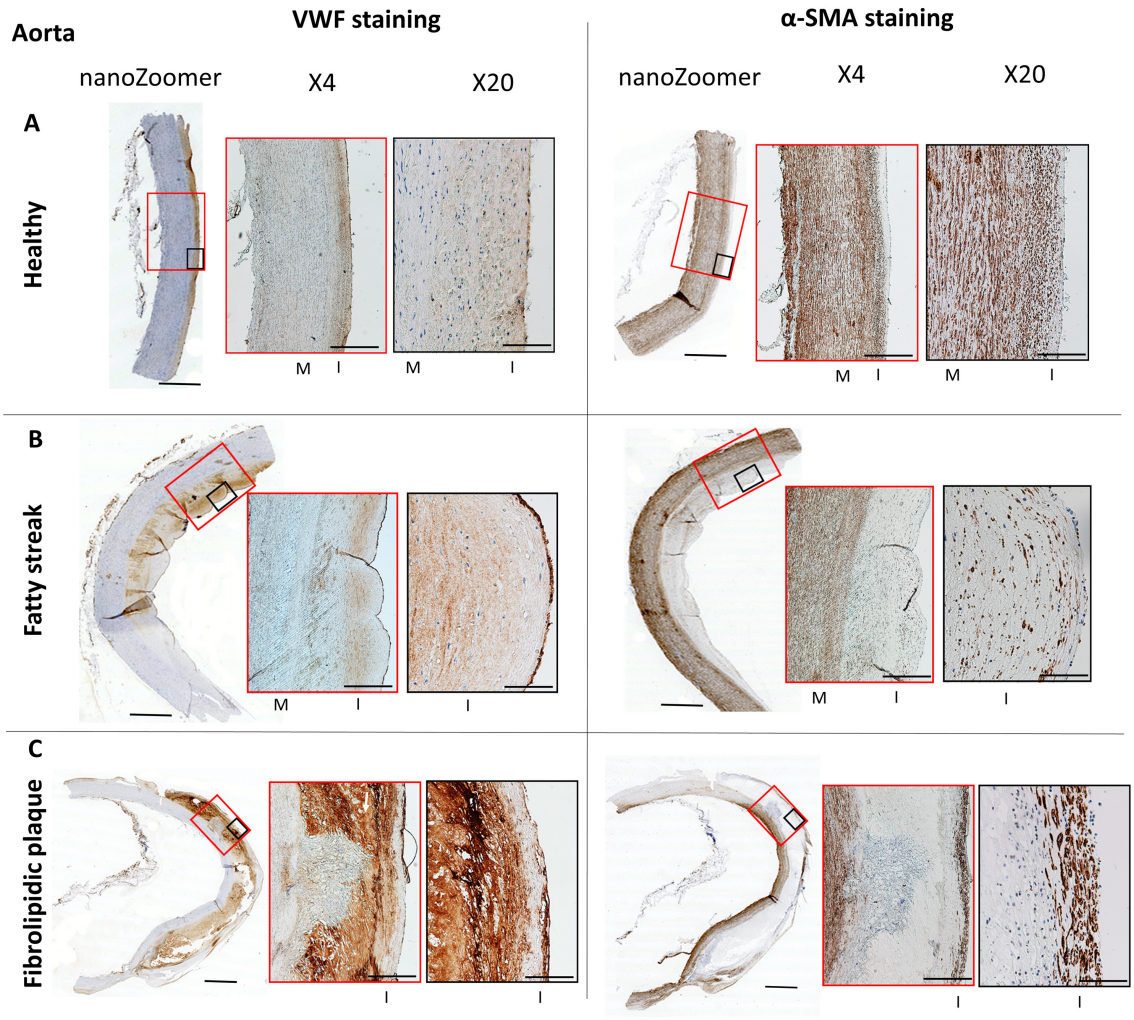
Aorta
VWF staining
α-SMA staining
nanoZoomer
X4
X20
nanoZoomer
X4
X20
A
Healthy
M
I
M
I
M
I
M
I
B
Fatty streak
M
I
I
M
I
I
C
Fibrolipidic plaque
I
I
I
I

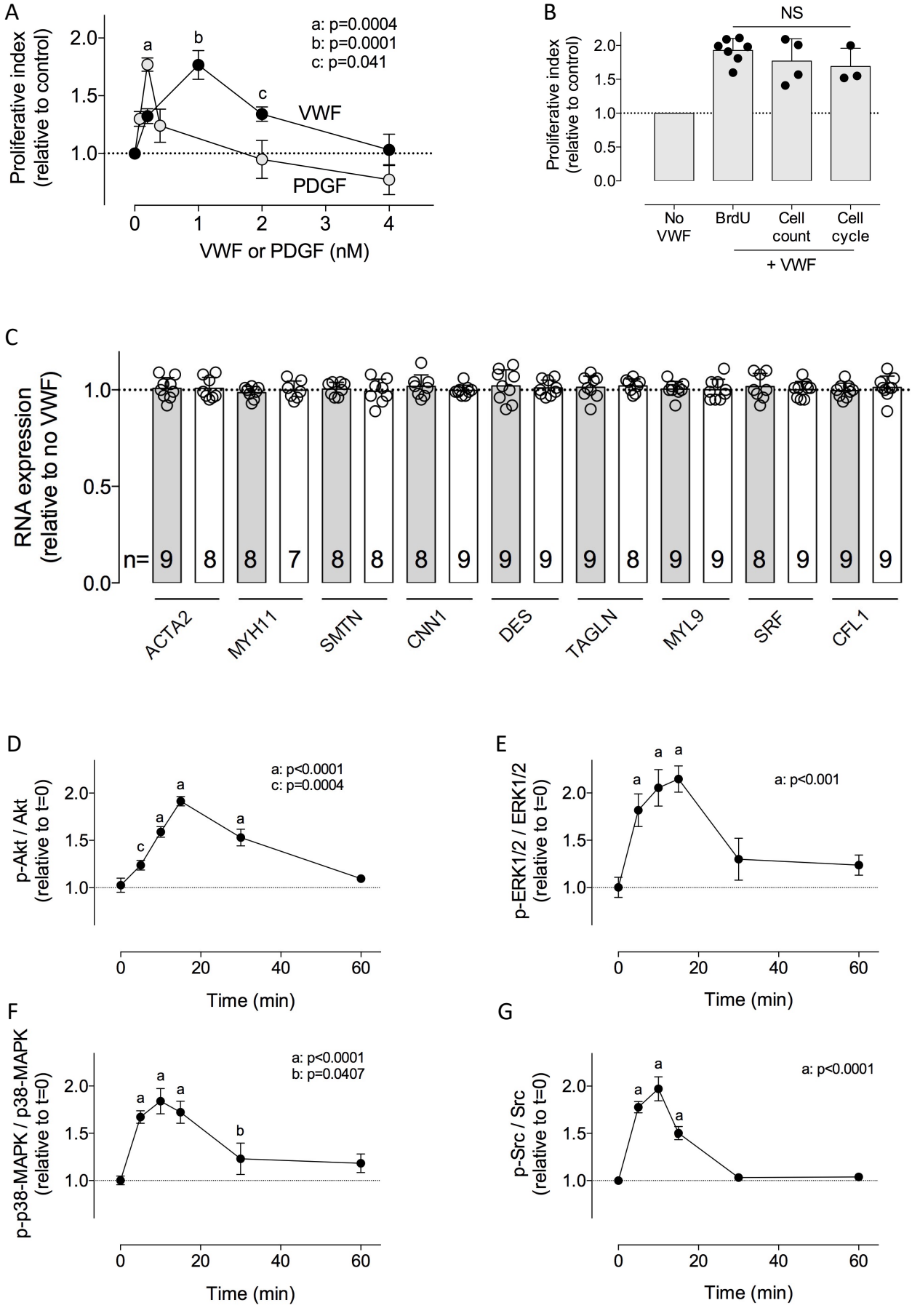
A
Proliferative index (relative to control)
a: p=0.0004
b: p=0.0001
c: p=0.041
VWF
PDGF
VWF or PDGF (nM)
B
NS
Proliferative index (relative to control)
No VWF
BrdU
Cell count
Cell cycle
+ VWF
C
RNA expression (relative to no VWF)
n= 9 8 8 7 8 8 8 9 9 9 9 8 9 9 8 9 9 9
ACTA2
MYH11
SMTN
CNN1
DES
TAGLN
MYL9
SRF
CFL1
D
p-Akt / Akt (relative to t=0)
a: p<0.0001
c: p=0.0004
Time (min)
E
p-ERK1/2 / ERK1/2 (relative to t=0)
a: p<0.001
Time (min)
F
p-p38-MAPK / p38-MAPK (relative to t=0)
a: p<0.0001
b: p=0.0407
Time (min)
G
p-Src / Src (relative to t=0)
a: p<0.0001
Time (min)

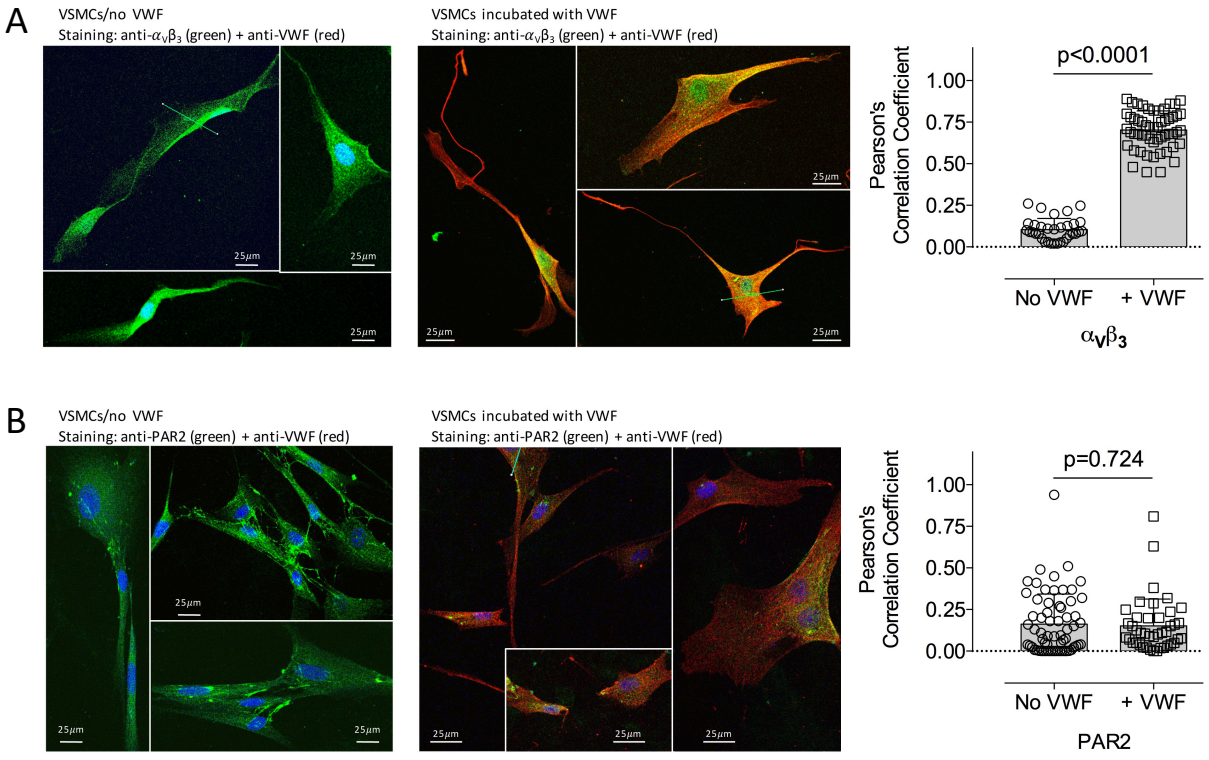
A
VSMCs/no VWF
Staining: anti-αvβ3 (green) + anti-VWF (red)
VSMCs incubated with VWF
Staining: anti-αvβ3 (green) + anti-VWF (red)
25µm
Pearson's Correlation Coefficient
p<0.0001
1.00
0.75
0.50
0.25
0.00
No VWF
+ VWF
αvβ3
B
VSMCs/no VWF
Staining: anti-PAR2 (green) + anti-VWF (red)
VSMCs incubated with VWF
Staining: anti-PAR2 (green) + anti-VWF (red)
Pearson's Correlation Coefficient
p=0.724
No VWF
+ VWF
PAR2

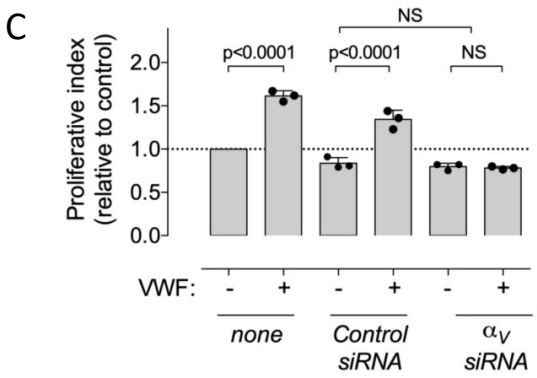
C
Proliferative index (relative to control)
NS
p<0.0001
p<0.0001
NS
2.0
1.5
1.0
0.5
0.0
VWF: - + - + - +
none
Control siRNA
αV siRNA

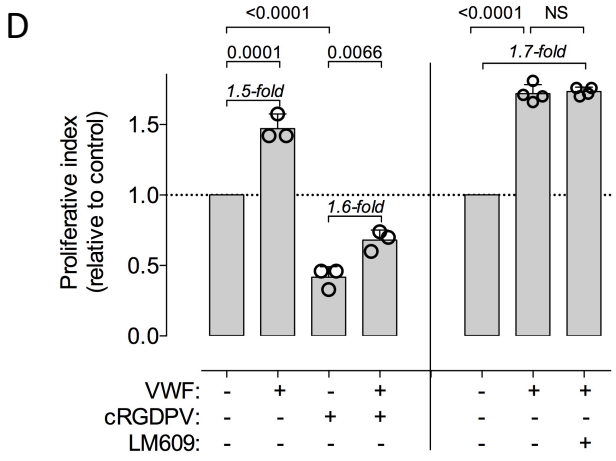
D
<0.0001
<0.0001
NS
0.0001
0.0066
1.7-fold
1.5-fold
1.6-fold
Proliferative index (relative to control)
1.5
1.0
0.5
0.0
VWF: - + - + - + +
cRGDPV: - - + + - - -
LM609: - - - - - - +

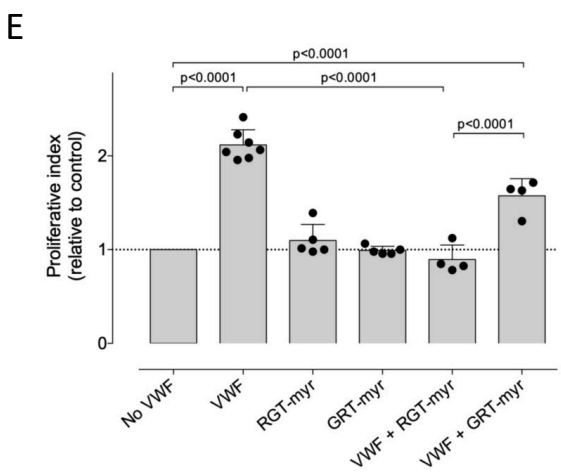
E
p<0.0001
p<0.0001
p<0.0001
p<0.0001
Proliferative index (relative to control)
2
1
0
No VWF
VWF
RGT-myr
GRT-myr
VWF + RGT-myr
VWF + GRT-myr

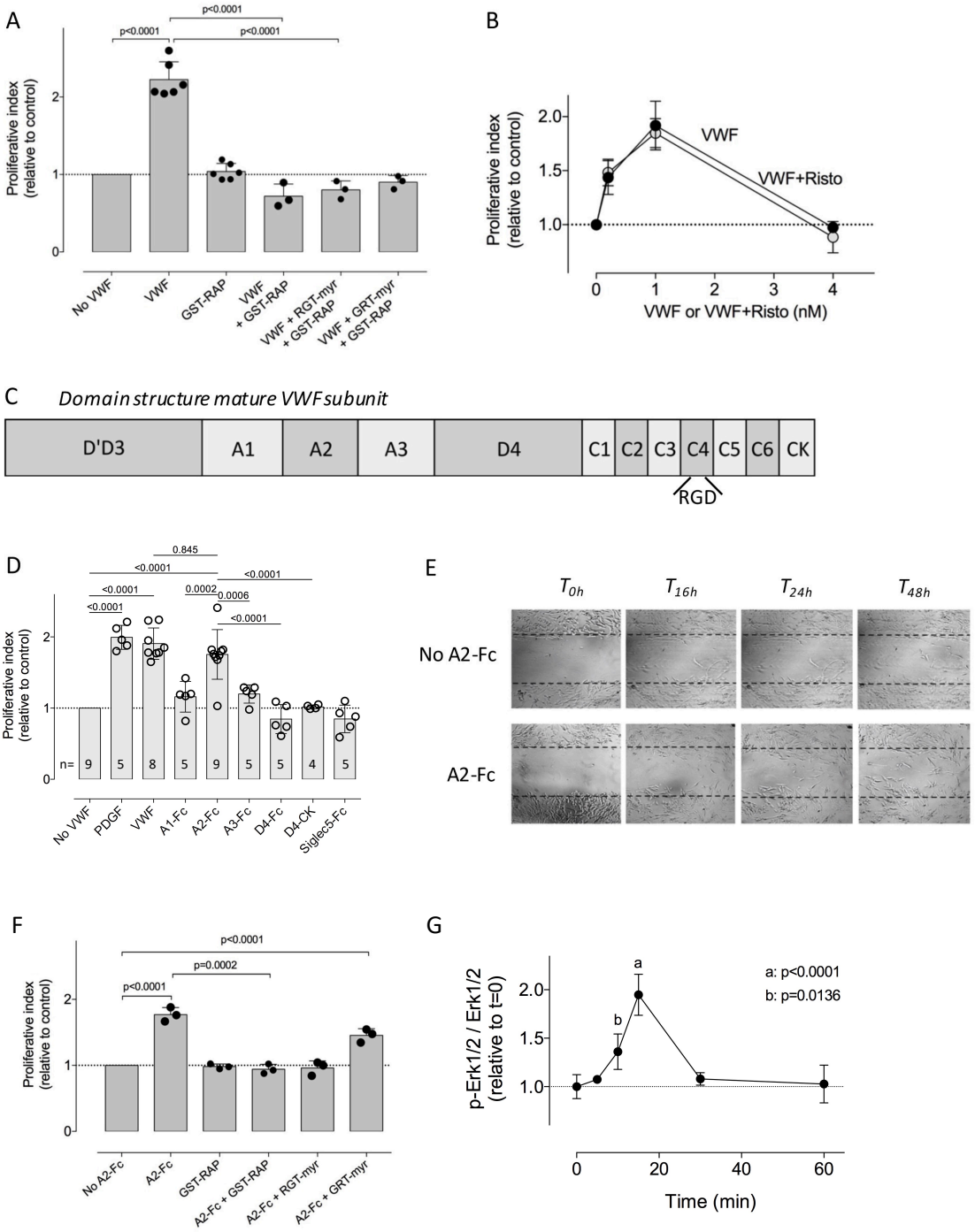
A
p<0.0001
p<0.0001
p<0.0001
Proliferative index (relative to control)
No VWF
VWF
GST-RAP
VWF + GST-RAP
VWF + RGT-myr + GST-RAP
VWF + GRT-myr + GST-RAP
B
Proliferative index (relative to control)
VWF
VWF+Risto
VWF or VWF+Risto (nM)
C
Domain structure mature VWF subunit
D'D3
A1
A2
A3
D4
C1
C2
C3
C4
C5
C6
CK
RGD
D
Proliferative index (relative to control)
n= 9 5 8 5 9 5 5 4 5
No VWF
PDGF
VWF
A1-Fc
A2-Fc
A3-Fc
D4-Fc
D4-CK
Siglec5-Fc
E
T0h
T16h
T24h
T48h
No A2-Fc
A2-Fc
F
Proliferative index (relative to control)
p<0.0001
p=0.0002
p<0.0001
No A2-Fc
A2-Fc
GST-RAP
A2-Fc + GST-RAP
A2-Fc + RGT-myr
A2-Fc + GRT-myr
G
p-Erk1/2 / Erk1/2 (relative to t=0)
a: p<0.0001
b: p=0.0136
Time (min)

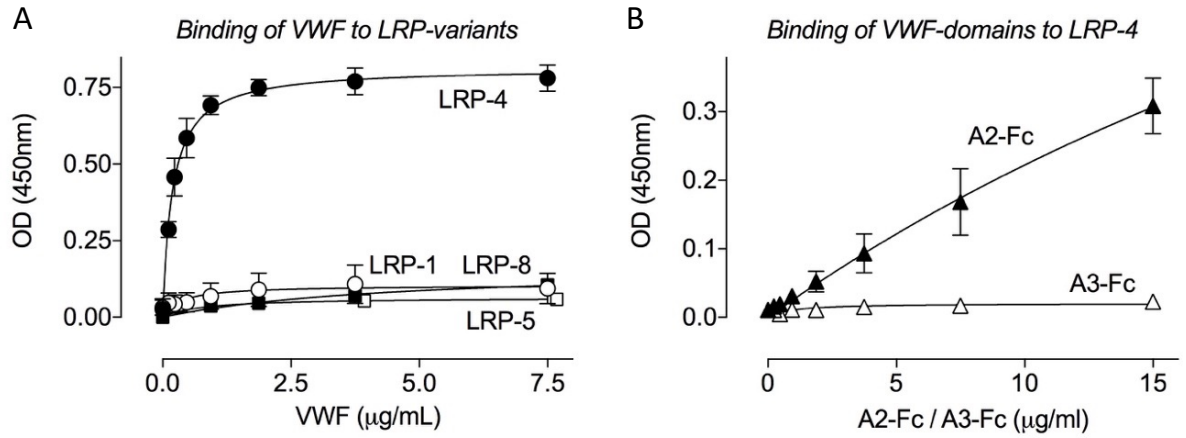
A
Binding of VWF to LRP-variants
OD (450nm)
0.75
0.50
0.25
0.00
LRP-4
LRP-1
LRP-8
LRP-5
0.0
2.5
5.0
7.5
VWF (µg/mL)
B
Binding of VWF-domains to LRP-4
OD (450nm)
0.3
0.2
0.1
0.0
A2-Fc
A3-Fc
0
5
10
15
A2-Fc / A3-Fc (µg/ml)

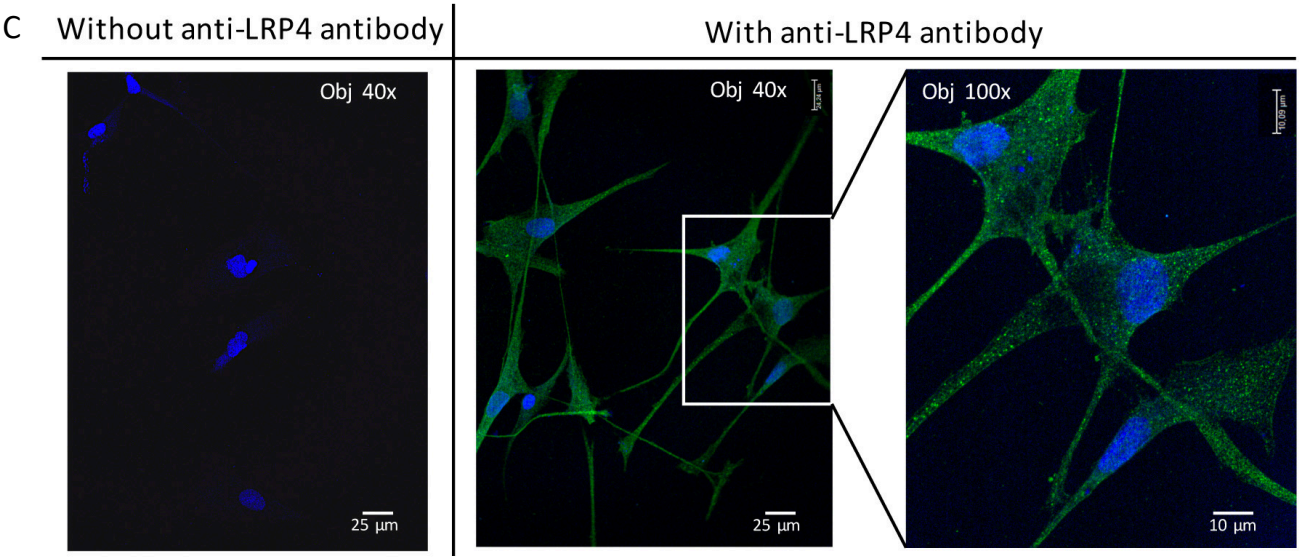
C
Without anti-LRP4 antibody
With anti-LRP4 antibody
Obj 40x
25 µm
Obj 40x
25 µm
Obj 100x
10 µm

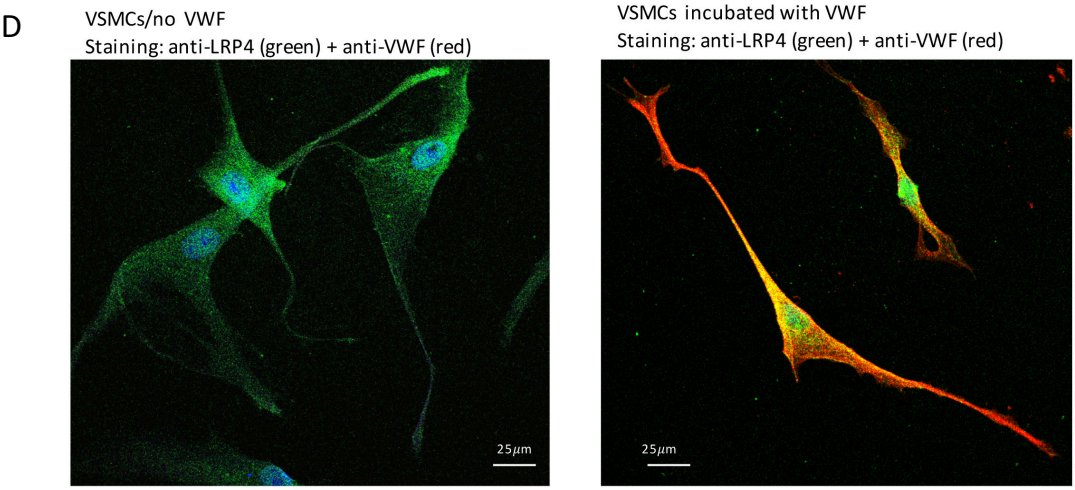
D
VSMCs/no VWF
Staining: anti-LRP4 (green) + anti-VWF (red)
25µm
VSMCs incubated with VWF
Staining: anti-LRP4 (green) + anti-VWF (red)
25µm

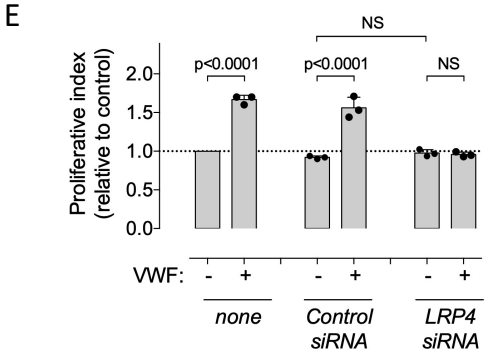
E
NS
p<0.0001
p<0.0001
NS
Proliferative index
(relative to control)
2.0
1.5
1.0
0.5
0.0
VWF:
-
+
-
+
-
+
none
Control
siRNA
LRP4
siRNA

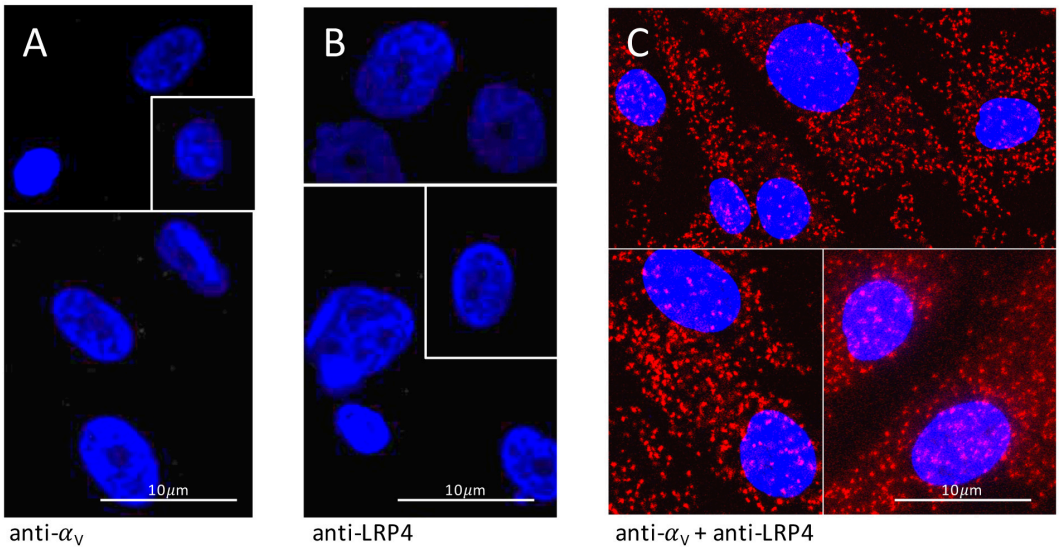
A
B
C
10μm
10μm
10μm
anti-αV
anti-LRP4
anti-αV + anti-LRP4

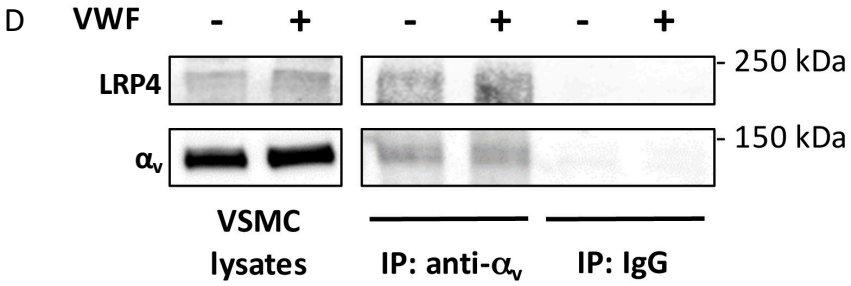
D
VWF - + - + - +
LRP4
αv
250 kDa
150 kDa
VSMC lysates
IP: anti-αv
IP: IgG

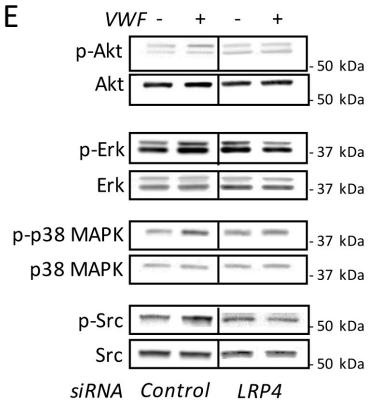
E
VWF - + - +
p-Akt
Akt
p-Erk
Erk
p-p38 MAPK
p38 MAPK
p-Src
Src
50 kDa
37 kDa
siRNA Control LRP4

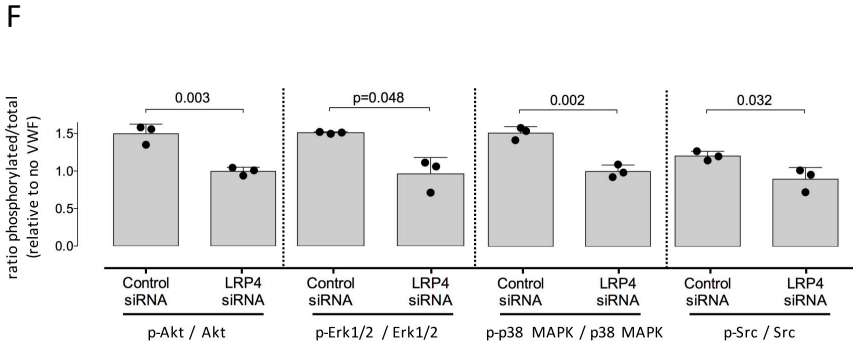
F
ratio phosphorylated/total (relative to no VWF)
0.003
p=0.048
0.002
0.032
Control siRNA
LRP4 siRNA
p-Akt / Akt
p-Erk1/2 / Erk1/2
p-p38 MAPK / p38 MAPK
p-Src / Src

Supplementary materials

Jérémy Lagrange[#1], Morel E. Worou[#1], Jean-Baptiste Michel[2], Alexandre Raoul[1], Mélusine Didelot[1], Vincent Muczynski[3], Paulette Legendre[3], François Plénat[4], Guillaume Gauchotte[5], Marc-Damien Lourenco-Rodrigues[3], Olivier D. Christophe[3], Peter J. Lenting[3], Patrick Lacolley[1], Cécile V. Denis*[3], Véronique Regnault*[1]

[1] INSERM, UMR_S 1116, Vandœuvre-lès-Nancy, France; Université de Lorraine, DCAC, Nancy, France.

[2] INSERM, UMR_S 1148, LVTS, Université de Paris, France

[3] HITh, UMR_S1176, INSERM, Université Paris-Saclay, 94276, Le Kremlin-Bicêtre, France

[4] Université de Lorraine, Nancy, France.

[5] CHRU, Anatomie et cytologie pathologiques, Nancy, France

1. Supplementary Tables and Figures

Supplementary Table 1

Carotid artery ligation model			
Mouse strain	Mice with hyperplasia (n)	Mice without hyperplasia (n)	
VWF+/+	5	4	*p*=0.015
VWF-/-	0	8	
Femoral artery denudation model			
Mouse strain	Mice with hyperplasia (n)	Mice without hyperplasia (n)	
VWF+/+	10	4	*p*=0.038
VWF-/-	4	9	

p-values were calculated using the N-1 Chi-square test.

Supplementary figure S1

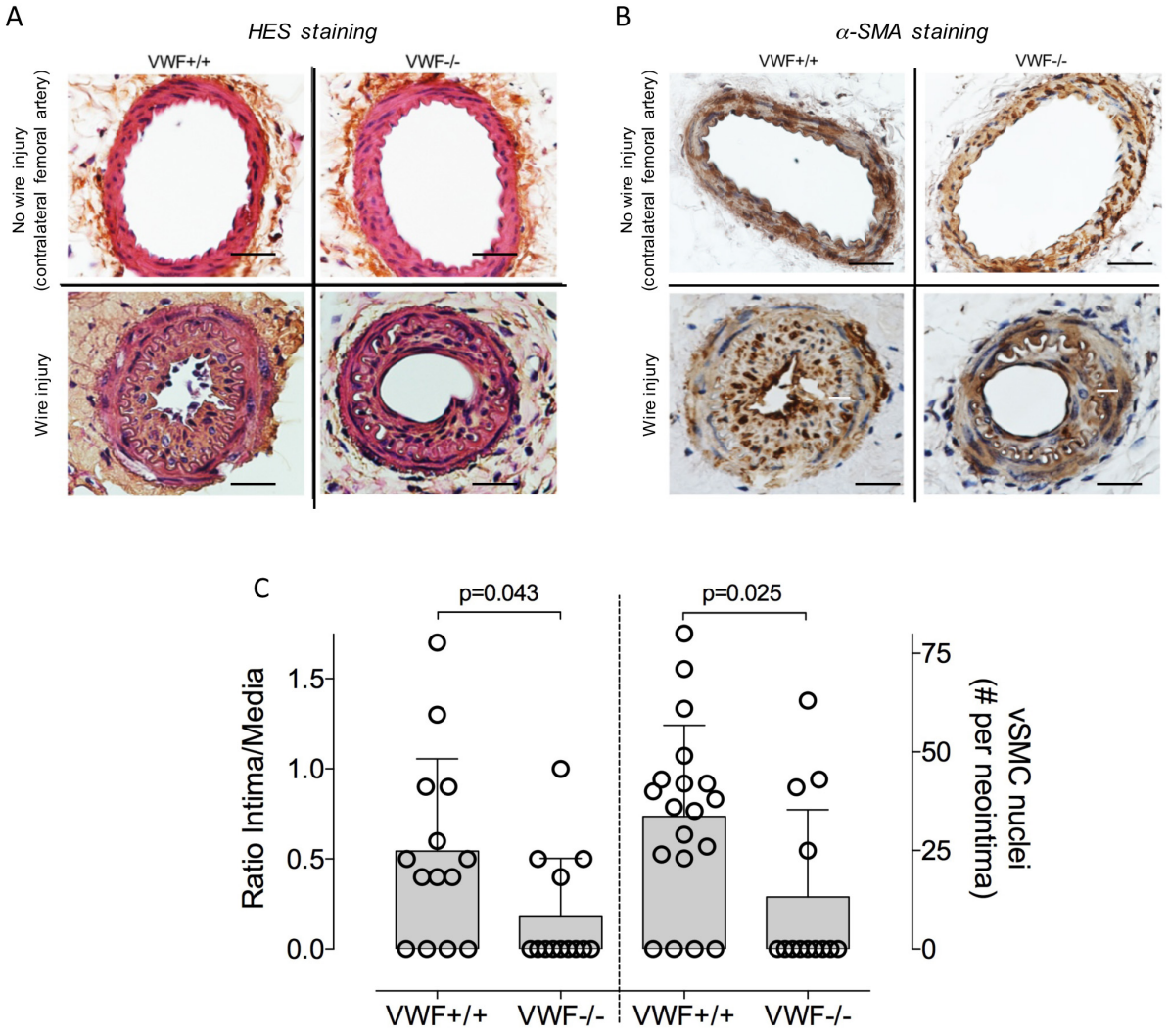

A-B. HES (panel A) and α-SMA (panel B) staining showing intimal hyperplasia in the femoral artery 4 weeks post injury in VWF+/+ and VWF-/- animals. Scale black bars, 50 µm. **C**. Intima/media ratio and nuclei count in injured femoral arteries (n=14 and 13 for VWF+/+ and VWF-/- mice respectively). Statistical analysis was performed using a Mann-Whitney test.

Supplementary figure S2

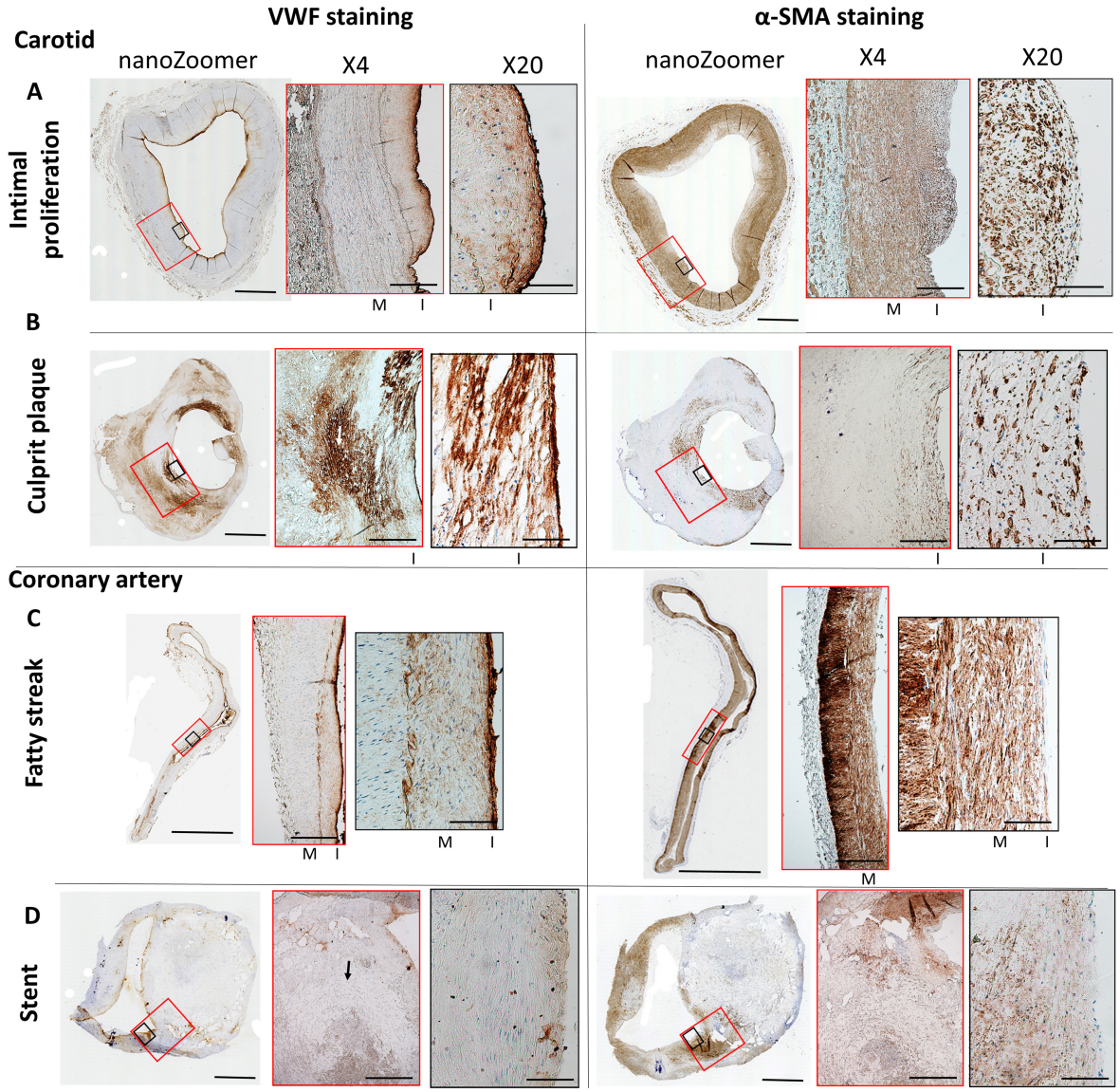

Immunostaining of VWF and α-SMA in different atherosclerotic stages of carotid and coronary arteries. **A.** Detection of VWF in endothelium and intimal proliferation (α-SMA-rich area) in primitive carotid artery. **B.** Culprit plaque (surgical endarteriectomy) showing VWF accumulation in the fibrocellular cap and in external intraplaque hemorrhagic areas (white arrow). **C.** VWF deposits in the α-SMA-positive neointima of coronary fatty streaks. **D.** Neo-atherosclerosis in area of coronary artery stenting showing VWF accumulation in the subendothelial α-SMA-rich area of the shoulder of the stented plaque (black arrow). Full morphology of the section (nanoZoomer) were associated with X4 magnification (red boxes) and X20 magnification (black boxes). M, media; I, intima. Scale bars: nanoZoomer: 2 mm; X4: 1 mm; X20: 0.2 mm.

Supplementary figure S3

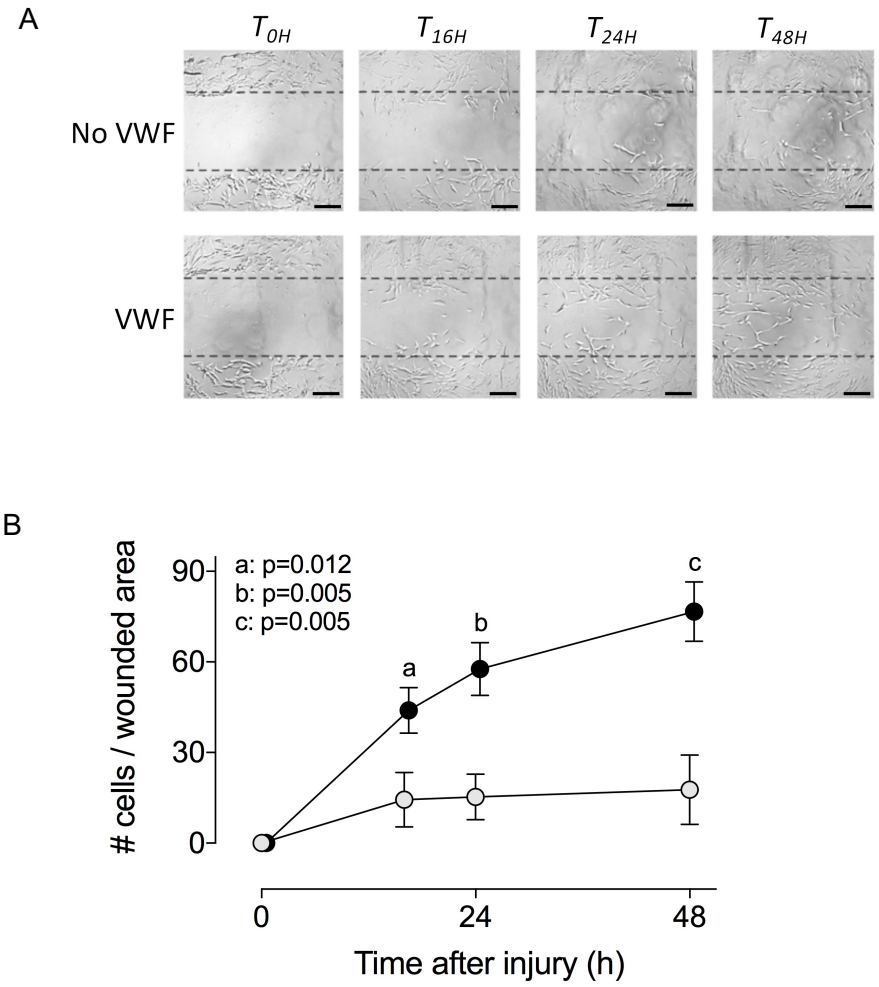

A wound healing scratch assay was performed on human VSMCs in the absence or presence of VWF (1 nM). Reappearance of cells in the wounded area was monitored at t=0,16, 24 and 48h (A) and quantified using ImageJ Software (B). Data represent mean±SD with n=3. Scale bars = 0.1 mm. Statistical analysis was performed using multiple t-test.

Supplementary figure S4

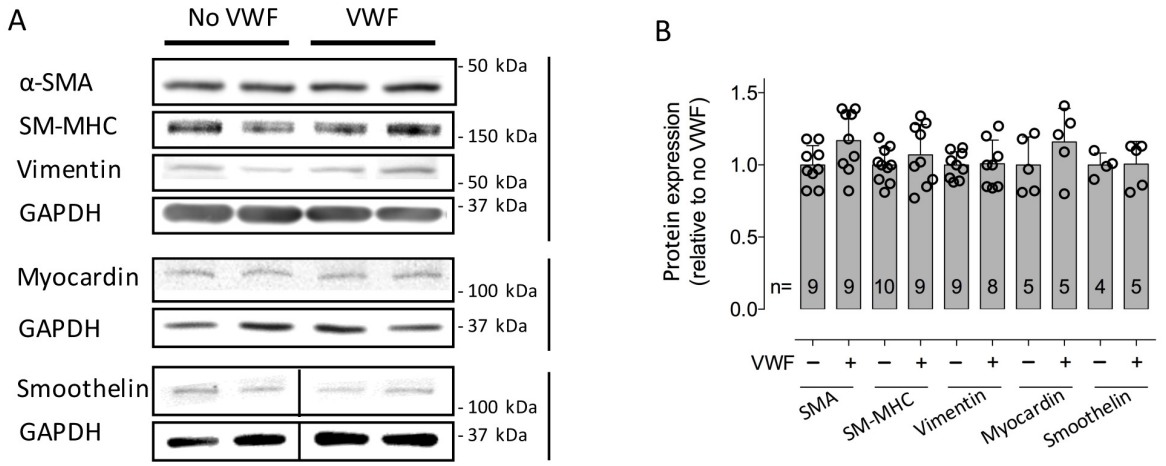

Expression of VSMC differentiation markers was analyzed following incubation with VWF (1 nM) for 24h via Western blotting of cell lysates using antibodies against α-SMA, vimentin, SM-MHC, myocardin or smoothelin. Data represent mean±SD, and n is indicated for each condition. Shown is the relative change in expression. Vertical bars next to panel A indicate bands analyzed on the same gels.

Supplementary figure S5

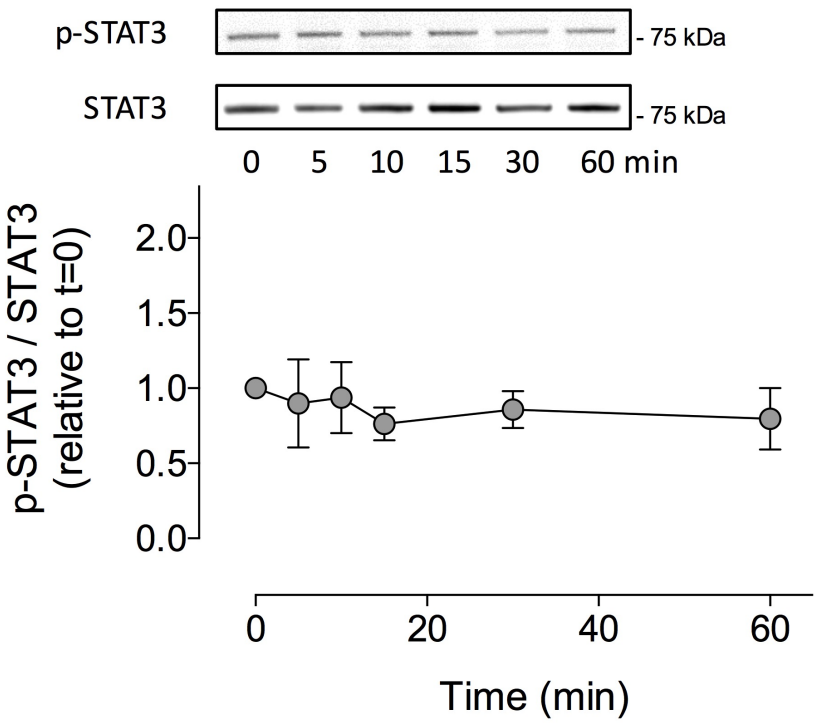

Phosphorylation of STAT3 was assessed after exposing cells to 1 nM VWF for 5 to 60 min. Cell lysates were prepared and phosphorylation of STAT3 (Tyr^{705}) was determined by Western blotting using primary rabbit antibodies (1/1000). Immunoreactive bands were visualized by chemiluminescence and quantified using a luminescent image analyzer system. Experiment was reproduced three times and results are expressed as fold increase relative to unstimulated control. Graph represents mean±SD (n=3). Statistical analysis was performed using one-way Anova with Dunnett's multiple comparison. No significant difference was measured at any time point.

Supplementary figure S6

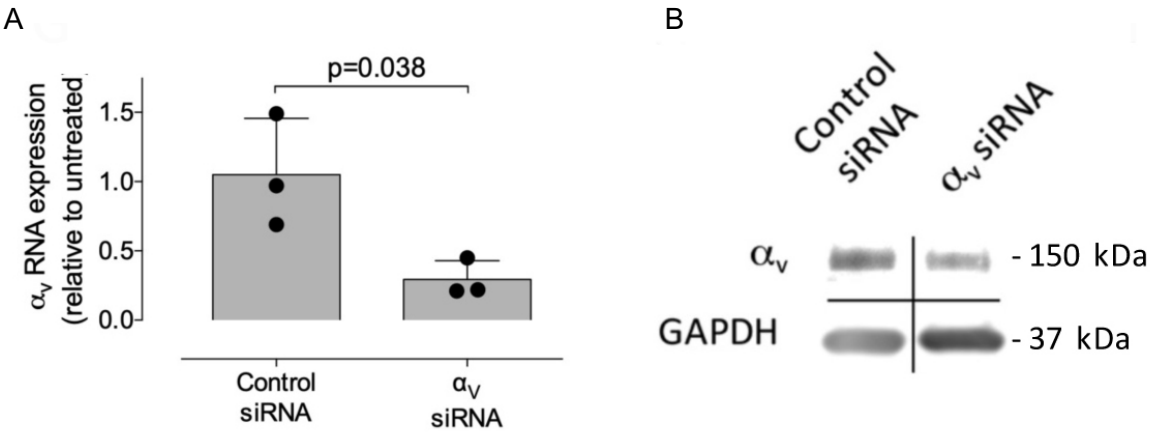

α_v residual RNA (A) or protein (B) expression in VSMCs following transfection with control or siRNA to α_v. Data represent mean±SD (n=3). Statistical analysis was performed using unpaired t-test.

Supplementary figure S7

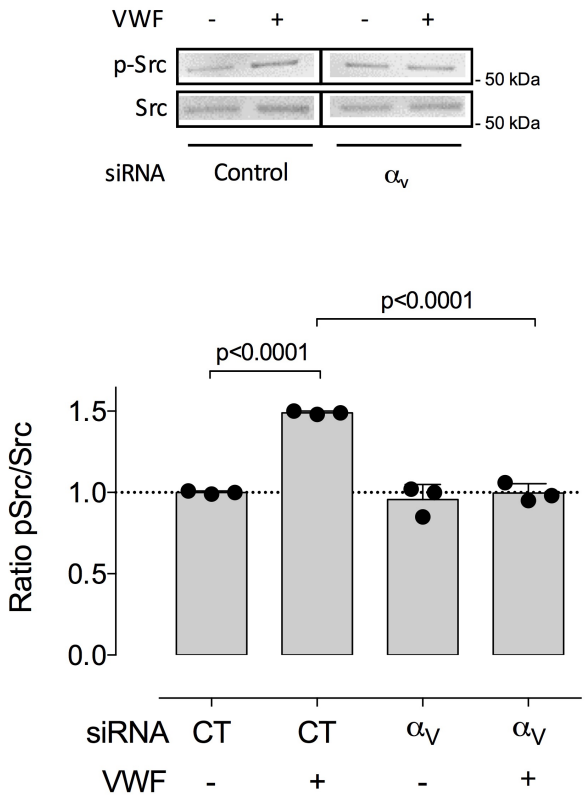

Phosphorylation of Src was assessed after exposing cells transfected with control siRNA or siRNA against α_v to 1 nM VWF for 15 min. Cell lysates were prepared and phosphorylation of Src (Tyr^{416}) was determined by Western blotting using primary rabbit antibodies (1/1000). Immunoreactive bands were visualized by chemiluminescence and quantified using a luminescent image analyzer system. Experiment was reproduced three times and results are expressed as fold increase relative to unstimulated control. Data represent mean±SD (n=3). Statistical analysis was performed using one-way Anova with Tukey's multiple comparison.

Supplementary figure S8

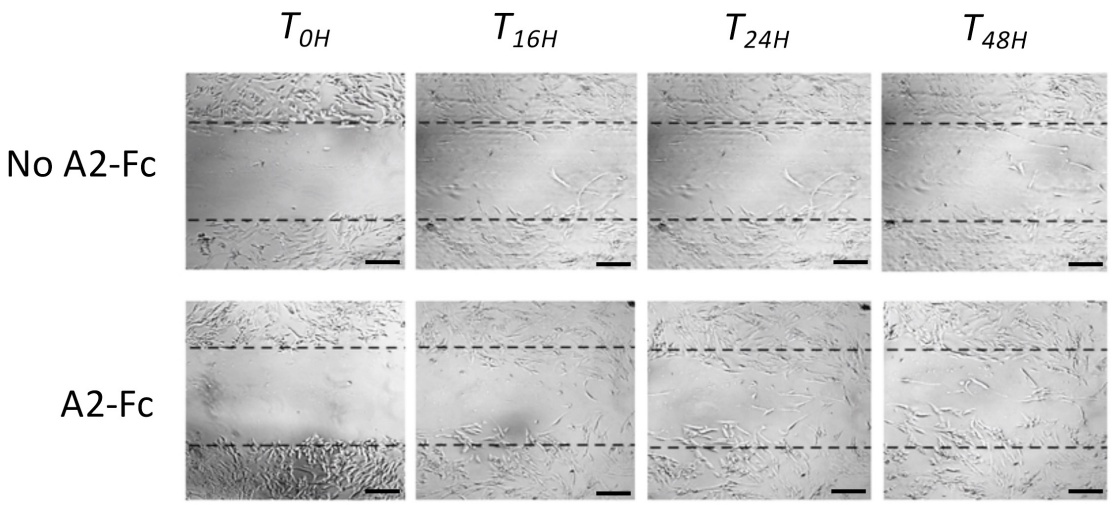

A wound healing scratch assay was performed on human VSMCs in the absence or presence of VWF-A2/Fc (100 ng/ml). Reappearance of cells in the wounded area was monitored at t=0,16, 24 and 48h and quantified using ImageJ Software. Scale bars= 0.1 mm.

Supplementary figure S9

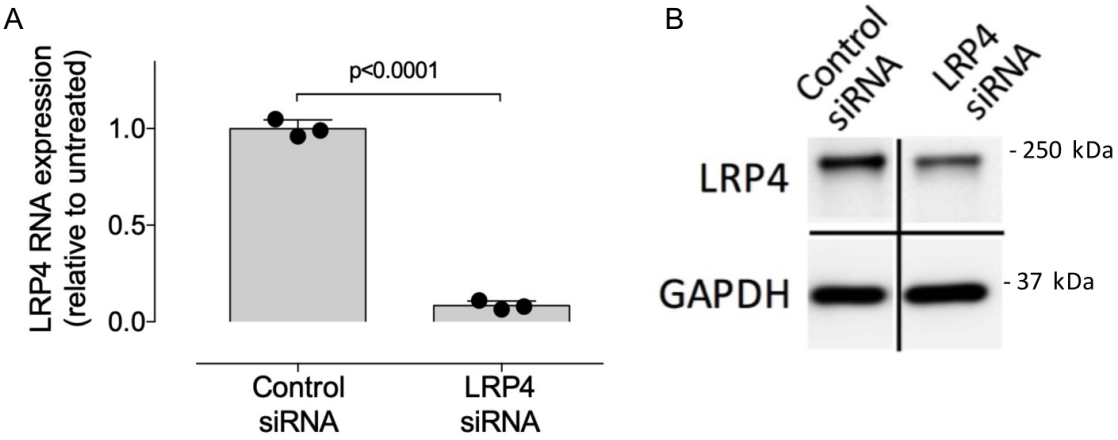

LRP4 residual RNA (A) or protein (B) expression in VSMCs following transfection with control or siRNA to LRP4. Statistical analysis was performed using unpaired t-test. Data represent mean±SD (n=3).

Supplementary figure S10

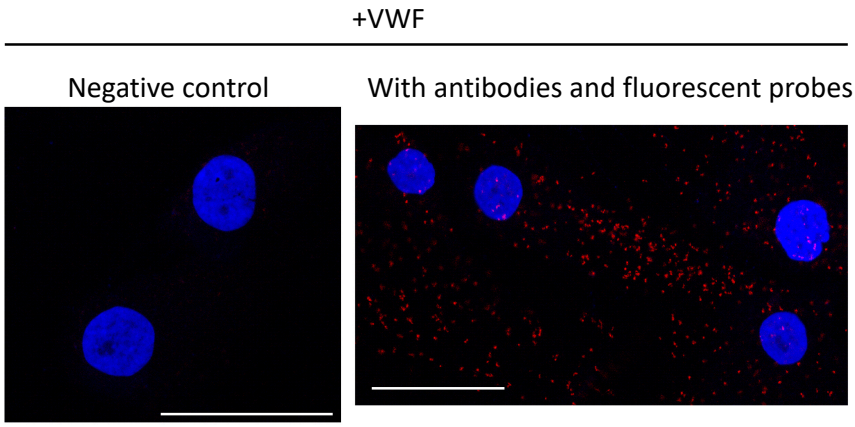

Duolink®-PLA analysis of LRP4 and $\alpha_v\beta_3$ expression and colocalization on VSMCs treated with VWF (1 nM). Left panel (negative control) represents conditions in the absence of fluorescent probes. Right panel represent test conditions with primary and secondary antibodies and fluorescent probes. Red spots appear only when LRP4 and $\alpha_v\beta_3$ are within a distance ≤40nm. Nuclei were counterstained with DAPI. Scale bars: 5 µM, Objective 63x.

2. Supplementary material and methods

2.1 Major Resources Tables

2.1.1 Reagents and cells

Name	Vendor or Source
Human aortic Vascular Smooth Muscle Cells	Lonza (Levallois-Perret, France)
Smooth Muscle Cell Growth Medium-2	Lonza (Levallois-Perret, France)
Recombinant human Platelet-derived growth factor	Bio-Techne (Lille, France)
Placenta-derived LRP1	BioMac (Leipzig, Germany)
Recombinant human LRP4	Bio-Techne
Recombinant human LRP8	Bio-Techne
Recombinant human LRP5	Novus Biologicals (Lille, France)
MATra-Si Reagent (Magnet Assisted Transfection)	Thermo Fisher Scientific (Illkirch-Graffenstaden, France)
BrdU Cell Proliferation Assay Kit	Cell Signalling Technologies (Saint Quentin en Yvelines, France)
Cell-based ELISA for detecting phospho-ERK1/2 ($pThr^{202}$/$pThr^{204}$) in cultured cell lines (RAB0350)	Sigma-Aldrich (Saint Quentin Fallavier, France)
Src (p-Tyr418) colorimetric cell-based ELISA kit (EKC1967)	Boster Bio/ Clinisciences (Nanterre, France)
Akt (p-Thr308) colorimetric cell-based ELISA kit (EKC2635)	Boster Bio/ Clinisciences (Nanterre, France)
P38-Mapk (p-Thr179/p-Tyr181) colorimetric cell-based ELISA kit (EKC2199)	Boster Bio/ Clinisciences (Nanterre, France)
Dynabeads Protein G-immunoprecipitation kit	Invitrogen

2.1.2 Antibodies

Name	Vendor or Source	Clone or reference
Immunostaining- primary antibodies		
Mouse monoclonal antibody against PCNA	Abcam (Paris, France)	ab29
Rabbit polyclonal antibodies against VWF	Dako	A0082
Pool of monoclonal antibodies to human von Willebrand factor	Home-made	
Mouse monoclonal antibody against PAR-2	Santa Cruz Biotechnology	Sc-13504
Mouse monoclonal antibody against human LRP4	Bio-Techne	MAB5948
Rabbit polyclonal antibodies to human $\alpha_v\beta_3$ integrin	Bioss Antibodies, Clinisciences	bs-1310F
Mouse monoclonal antibody against human $\alpha_v\beta_3$ integrin	Merck (Fontenay-sous-Bois, France),	MAB1976/Clone LM609
Rabbit monoclonal antibody against α_V	Abcam (Paris, France)	Ab179475
Normal rabbit IgG	Sigma-Aldrich	I8140
Secondary antibodies		
Secondary horseradish peroxidase (HRP)-linked antibodies	GE Healthcare Life Sciences (Velizy-Villacoublay, France)/Abcam	

Secondary fluorescent antibodies	GE Healthcare Life Sciences	
Secondary biotinylated antibodies	Agilent Technologies	
Anti Fc-HRP	Sanquin (Amsterdam, The Netherlands)	A5228
Mouse monoclonal antibody against human vimentin	Agilent Technologies (Les Ulis, France)	M0725
Duolink®-Proximity Ligation Assay (Duolink®-PLA) In Situ kit	Sigma Aldrich (Saint Quentin Fallavier, France)	
Differentiation-related antibodies		
Rabbit polyclonal antibodies to Smooth Muscle Myosin Heavy Chain (SM-MHC)	Abcam (Paris, France)	ab125884
Rabbit polyclonal antibodies to Myocardin	Abcam (Paris, France)	ab107301
Rabbit polyclonal antibodies to Smoothelin	Abcam (Paris, France)	ab219652
Mouse monoclonal antibody to human α-SMA	Leica Biosystems (Newcastle, UK)	NCL-L-MSA/Clone alpha SM-1
Goat polyclonal antibodies to vimentin	Santa Cruz Biotechnology	Sc-25778
Rabbit polyclonal antibodies to GAPDH	Clinisciences (Nanterre, France)	sc-25778
Signaling-related antibodies		
Rabbit monoclonal antibody to p-ERK1/2	Cell Signaling Technologies,	D13.14.4E
Rabbit monoclonal antibody to total ERK1/2	Cell Signaling Technologies	137F5
Rabbit monoclonal antibody to p-p38-MAPK	Cell Signaling Technologies	3D7
Rabbit polyclonal antibodies to p38-MAPK	Cell Signaling Technologies	9212
Rabbit polyclonal antibodies to p-Akt	Cell Signaling Technologies	9275
Rabbit polyclonal antibodies to total Akt	Cell Signaling Technologies	9272
Rabbit polyclonal antibodies to Src	Cell Signaling Technologies	21085
Rabbit polyclonal antibodies to p-Src	Cell Signaling Technologies	2101
Rabbit polyclonal antibodies to pSTAT3	Cell Signaling Technologies	9145
Mouse monoclonal antibody against STAT3	Cell Signaling Technologies	124H6

2.1.3 Inhibitors

Name	Vendor or Source	Target
LRPAP1 (RAP or receptor associated protein)	Abcam	Pan-LRP inhibitor
Synthetic myristoylated RGT peptide	GL Biochem (Shanghai, China)	Inhibitor of outside-in signaling mediated by β3 integrin subunit

Synthetic myristoylated control GRT peptide	GL Biochem	Control peptide
Short interfering RNA (siRNA) against human LRP4	GeneCust (Ellange, Luxembourg)	Inhibitor of LRP4 expression
Short interfering RNA (siRNA) against human α_v	GeneCust	Inhibitor of α_v expression
Cyclic RGDPV peptide	Bachem (Bubendorf, Switzerland)	Inhibitor of $\alpha_v\beta_3$ ligand binding

2.1.4 Sequences

Name	Sequence
Short interfering RNAs (siRNA) against human LRP4 (5'-3')	5'-GCA AAG UAC UGA UCA ACA A 5'-GCU ACU GGC AUG AGU GAA A 5'-UGG AAG GAC UCA UGG AUA U
siRNAs against human α_v (5'-3')	5'-GCC AGC CAA UUG AAU UUG ATT 5'-GGC UGU CGG AGA UUU CAA UTT 5'-CCC AGU UGU AUC UCA CAA ATT
Control siRNA (5'-3')	5'-UUC UCC GAA CGU GUC ACG UTT
Forward primer ACTA2	5'-ACTGCCTTGGTGTGTGACAATGG
Reverse primer ACTA2	5'-TGGTGCCAGATCTTTTCCATG
Forward primer MYH11	5'-GGAGGATGAGATCCTGGTCA
Reverse primer MYH11	5'-TTAGCCGCACTTCCAGTTCT
Forward primer SMTN	5'-GGCAGTGTCACTCACGTCAC
Reverse primer SMTN	5'-CTGATCCAGCATCTTGTCCA
Forward primer CNN1	5'-ACATTTTTGAGGCCAACGAC
Reverse primer CNN1	5'-CTCCCACGTTCACCTTGTTT
Forward primer DES	5-CTGAGCAAAGGGGTTCTGAG
Reverse primer DES	5'-TGGCAGAGGGTCTCTGTCTT
Forward primer TAGLN	5'-AAGAATGATGGGCACTACCG
Reverse primer TAGLN	5'-ATGACATGCTTTCCCTCCTG
Forward primer MYL9	5'-ATGTTTGGGGAGAAGCTGAA
Reverse primer MYL9	5'-CCGGTACATCTCGTCCACTT
Forward primer SRF	5'-ATCTGGGACAGTGCAGATCC
Reverse primer SRF	5'-GCGGATCATTCACTCTTGGT
Forward primer CFL1	5'-GCAAGAAGGAGGATCTGGTG
Reverse primer CFL1	5'-GCTTGATCCCTGTCAGCTTC
Forward primer GAPDH	5'-CAGCCTCAAGATCATCAGCA
Reverse primer GAPDH	5'-TGTGGTCATGAGTCCTTCCA
Forward primer RPS29	5'-AAGATGGGTCACCAGCAGCTGTACTG
Reverse primer RPS29	5'-AGACACGACAAGAGCGAGAA

2.1 Proteins

Plasma-derived VWF was purified from concentrates (Wilfactin, LFB-Biomédicaments, Les Ullis, France) via size separation-chromatography[1]. VWF A1-Fc, A2-Fc, A3-Fc and D4-Fc include VWF residues 1261-1478, 1480-1672, 1681-1878 and 1947-2301, respectively. Proteins were expressed in BHK-cells using the pFuse-plasmid containing a C-terminal sequence of human IgG1 and were dimeric. Fc-tagged

proteins were purified to homogeneity using protein A-sepharose as instructed by the manufacturer (VWF International, Fontenay-sous-Bois, France). Fragment VWF/A1-CK (containing residues 1260-2813 with a N-terminal His-tag) was expressed and purified as described[1].

2.2 Mouse model of femoral artery wire injury

IH was investigated in VWF+/+ and VWF-/- mice using an established neointima formation model of femoral artery wire injury[2]. Briefly, anesthesia was induced by isoflurane inhalation at 3.5% in 1L/min oxygen, and then maintained at 1.5% in 1L/min oxygen during the intervention. After a skin incision, the left femoral artery was isolated under surgical microscope. An arteriotomy was made distal to the epigastric branch, and a 0.35-mm diameter angioplasty guide wire (Abbott Vascular, France) was inserted and pushed three times within the vessel until the aortic bifurcation and removed. The arteriotomy site was then ligated with an 8-0 nylon suture and the incision closed. The right non-operated contralateral femoral artery was used as control. At 4 weeks post-surgery, mice were euthanized via exsanguination under isoflurane anesthesia (1.5% in 1L/min oxygen) in order to collect femoral arteries. Neointimal formation was evaluated by histological analysis.

2.3 Mouse model of carotid artery ligation

Carotid ligation model was performed in VWF+/+ and VWF-/- mice. Anesthesia was induced by isoflurane inhalation. The neck was epilated and disinfected. An incision was made longitudinally in the neck. The left common carotid artery was exposed by blunt dissection. The vessel was ligated with a 6.0 silk suture. At 4 weeks post-surgery, mice were euthanized via exsanguination under isoflurane anesthesia (1.5% in 1L/min oxygen) in order to collect the left common artery as well as the right common carotid as control.

2.4 Tissue processing and histological analysis

At the time of euthanasia, femoral arteries or carotids were exposed and fixed *in situ* with Bouin's fluid for 30 min. The vessels were then harvested and immersed in the same fixative for 24h. Fixed specimens were embedded in paraffin following regular procedures. Five µm thick sections were stained with Hematoxylin-Eosin-Saffron (HES) for morphometric analysis.

2.5 Morphometric analysis and intimal hyperplasia quantification

The HES-stained sections images were examined for the extent of neointimal formation. The luminal, intimal and medial areas of each section were calculated by encircling the lumen edge, internal and external elastic lamina, respectively, using a Nikon's NIS Elements Basic Research microscope imaging software. The intima-to-media (I/M) ratio was calculated as described[3]. Nuclei from the neointima were counted in mice displaying neointimal hyperplasia after femoral artery injury or common carotid ligation.

2.6 Flow cytometry

Cell cycle progression was determined by propidium iodide (PI, Sigma Aldrich, Saint Quentin Fallavier, France) staining using flow cytometry. Cells were fixed with 70% cold ethanol at 4°C overnight. Then, cells were rehydrated and washed twice with ice-cold PBS, and incubated with 10 mg/ml RNase (Sigma) at 37°C. Cell cycle was monitored by using PI staining of nuclei (50 µg/ml). Stained samples were analyzed on a flow cytometer (Gallios-Kalusa software Beckman Coulter). A minimum of 10,000 events were collected. Doublets and aneuploid cells were excluded.

2.7 Immunofluorescence staining of VSMCs

VSMCs were grown on glass coverslips and fixed with 4% (w/v) buffered formaldehyde solution prepared by depolymerization of paraformaldehyde. After blocking of non-specific binding sites with PBS-tween-20, 5% BSA for 30 min, primary antibodies directed against VWF, $\alpha_v\beta_3$ integrin or LRP4 were incubated 2h at RT in PBS/BSA (1%) and secondary antibodies were incubated 1h at RT. Nuclei were counterstained with 1 µg/mL of 4',6'-diamidino-2-phenylindole (DAPI) and coverslips were mounted with Prolong Gold antifade reagent (Life Technologies) and stored at -20°C. Negative controls were performed by omitting the primary antibody or the VWF treatment.

For confocal microscopy, images were acquired using a scanning laser confocal Leica TCS SP5 X with a 40x water objective lens. Images were acquired using stacks (1 µm steps) in sequential for the three channels (488, 555 & 633 nm). Images were analyzed by Image J software using the plugin *colocalization finder* which calculated the Pearson's coefficient based on mean pixel intensity. Cells were marked as regions of interest (ROIs) in the images. Using the ROI scatterplot of the plugin we subtracted the

background and measured the Pearson's coefficient. Values in the range [-1, 1], are obtained using this test with 0 indicating that there is no discernable correlation and -1 and +1 meaning strong negative or positive correlations[4].

For the Duolink®- Proximity Ligation Assay (PLA) to detect close proximity between different proteins, double immunostaining of human VSMCs (treated or not with VWF) was performed using primary antibodies to LRP4 and $\alpha_v\beta_3$ integrin, the secondary antibodies being replaced by PLA probes. The remainder of the protocol was conducted according to the manufacturer's recommendations using the 550 nm wavelength detection kit. Hybridization between the two PLA probes leading to the fluorescent signal only occurs when the distance between the two detected antigens is less than 40 nm. For confocal microscopy, a Nikon C2 microscope with Ti-FL stage and C-HGFi fluorescent bulb was used. Acquisition was performed with the NiS Elements software.

2.8 Immuno-precipitation experiments

Equal amounts of VSMC-lysate (100 μg protein) were incubated with the rmonoclonal rabbit anti-α_V integrin antibody (Abcam, ab179475) or with normal rabbit IgG (Sigma-Aldrich, I8140). Protein/antibody complexes were then immunoprecipiated using the Dynabeads Protein G-immunoprecipitation kit (Invitrogen).

2.9 Quantitative PCR of cell-differentiation markers

Total RNA was extracted from VSMCs using the RNeasy Mini kit (Qiagen, Les Ulis, France). First strand cDNA was synthesized according to the manufacturer's instructions (Fermentas; Thermo-Fisher Scientific). Quantitative real-time PCR analysis was then performed using SYBR green PCR technology (Bio-Rad, Hercules, CA, USA). Sequence of the primers have been listed in Supplementary table 2.1.4.

3. Supplementary references

1. Lenting PJ, Westein E, Terraube V, Ribba AS, Huizinga EG, Meyer D, de Groot PG, Denis CV. An experimental model to study the in vivo survival of von Willebrand factor. Basic aspects and application to the R1205H mutation. *J Biol Chem* 2004;**279**:12102-12109.
2. Roque M, Fallon JT, Badimon JJ, Zhang WX, Taubman MB, Reis ED. Mouse model of femoral artery denudation injury associated with the rapid accumulation of adhesion molecules on the luminal surface and recruitment of neutrophils. *Arterioscler Thromb Vasc Biol* 2000;**20**:335-342.

3. Smirnova NF, Gayral S, Pedros C, Loirand G, Vaillant N, Malet N, Kassem S, Calise D, Goudouneche D, Wymann MP, Hirsch E, Gadeau AP, Martinez LO, Saoudi A, Laffargue M. Targeting PI3Kgamma activity decreases vascular trauma-induced intimal hyperplasia through modulation of the Th1 response. *J Exp Med* 2014;**211**:1779-1792.
4. French AP, Mills S, Swarup R, Bennett MJ, Pridmore TP. Colocalization of fluorescent markers in confocal microscope images of plant cells. *Nat Protoc* 2008;**3**:619-628.